AN INVESTIGATION OF THE AUTOIGNITION OF A COMBUSTIBLE MIXTURE DUE TO THE PRESENCE OF A HEATED SURFACE

Thesis by

Glenn August Schurman

In Partial Fulfillment of the Requirements

For the Degree of

Doctor of Philosophy

California Institute of Technology

Pasadena, California

1950

ACKNOWLEDGEMENTS

The author expresses his sincere appreciation to Dr. Peter Kyropoulos, who directed the research, and whose encouragement, enthusiasm, and aid made this investigation possible. Dr. Oliver Wulf gave a great deal of time and many helpful suggestions during the course of the work. Dr. David S. Wood also contributed many helpful suggestions. The author takes this opportunity to thank Prof. George R. MacMinn for his suggestions regarding the composition of the manuscript. Mr. Charles F. Quirmbach was of great assistance in preparing the curves and figures.

ABSTRACT

An experimental investigation regarding the nature of the hydrogen-oxygen reaction in the vicinity of a heated surface is described. The experimental work was conducted at atmospheric pressure in a shallow rectangular combustion chamber. The upper surface of this chamber is heated to temperatures ranging from room temperature to 1615° R; the lower surface is maintained at a constant temperature of 550° R. The temperature distribution of the mixture between the two plates is the primary experimental measurement. This measurement was made with a Mach-Zehnder optical interferometer. The maximum temperature of the upper plate at which experiments were made was 1615° R. The maximum temperature at which interferograms were taken was limited by the presence of a nonuniform temperature distribution along the light path. It was found that the central area of the heated surface of the combustion chamber could be held at a temperature of 1710° R without an explosion occurring. The chemical reaction could not be detected below an upper plate temperature of 1500 ± 10° R. There is evidence that large composition gradients exist in the combustion chamber. These gradients persist for a much longer time than that predicted from the diffusion theory. Accordingly, the overall rate at which the reactants combine is much lower than that expected. The exact reasons for the suppression of the explosion and the reduced reaction rate are not understood. Two possible explanations are suggested.

TABLE OF CONTENTS

LIST OF FIGURES

LIST OF FIGURES (Continued)

I. INTRODUCTION

A great deal of work and thought has been given to the mechanism of chemical reactions. This field of investigation has become known as "Reaction Kinetics".

Early work concerning the chemical reactions of gaseous mixtures (about 1900) was centered mainly on determining explosion limits and rates of the various reactions as functions of the temperature and total pressure on the system. The only theory regarding the nature of the reaction at this time was the following rate equation. This equation is written symbolically as follows (1)*. In a reaction where $\alpha A + \beta B + \cdots = \gamma Y + \xi Z + \cdots$, the reaction rate is given by the expression

$$w = -\frac{dA}{dt} = -\frac{\beta}{\alpha}\frac{dB}{dt} = k\left[A\right]^{\alpha}\left[B\right]^{\beta}\cdots$$

where w is the reaction velocity, k is a function of the temperature only, and the square brackets indicate the concentration of the reactants or products. In principle, the reverse reaction should also be considered, but in the case of reactions which are strongly exothermic the reverse reaction is usually neglected. This theory is often referred to in the literature as the "Thermal Theory of Reaction".

In this work, a great many anomalous effects were found and it became evident that by the thermal theory alone many of the phenomena

---

*The figures appearing in parenthesis refer to the references listed at the end of this thesis.

could not be explained.

For example, one of the first modern investigations on the hydrogen and oxygen reaction was done by Bodenstein (2) in 1899. These tests were to determine the reaction rates of hydrogen-oxygen mixtures at various temperatures. The experiments were conducted by passing a mixture of hydrogen and oxygen through porcelain tubes with different volume to surface ratios. It was found that the reaction velocity in each tube could be expressed by the preceding relation, but the value of k varied greatly from vessel to vessel. Thus, it appeared that a surface reaction was predominating, and the simple relation was not generally applicable since the reaction was mainly catalytic.

Later work by Falk (3) and Dixon (4, 5) established the explosion limit of hydrogen-oxygen reaction as a function of temperature and pressure. The curve they found is shown schematically in Fig. 1. The segment AB is called the first explosion limit, the segment BC is called the second explosion limit, and the segment CD is called the third explosion limit. The inadequacy of the thermal theory can be best observed by comparing this curve to a curve predicted by the thermal theory (Fig. 2). As shown, the segments AB and CD might be explained by the thermal theory, but the segment BC is incompatible with this theory.

Thus it is evident that the process is more complicated than the simple combination of hydrogen with oxygen to produce water.

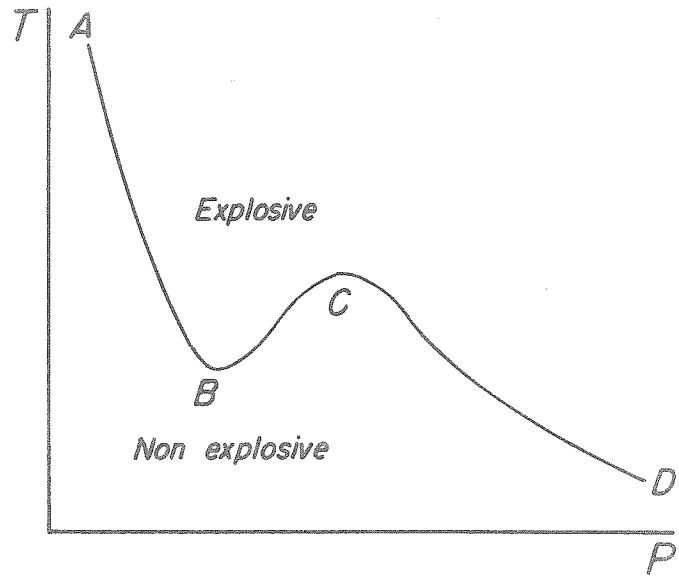

FIGURE 1

Typical explosion limit for branching chain reaction

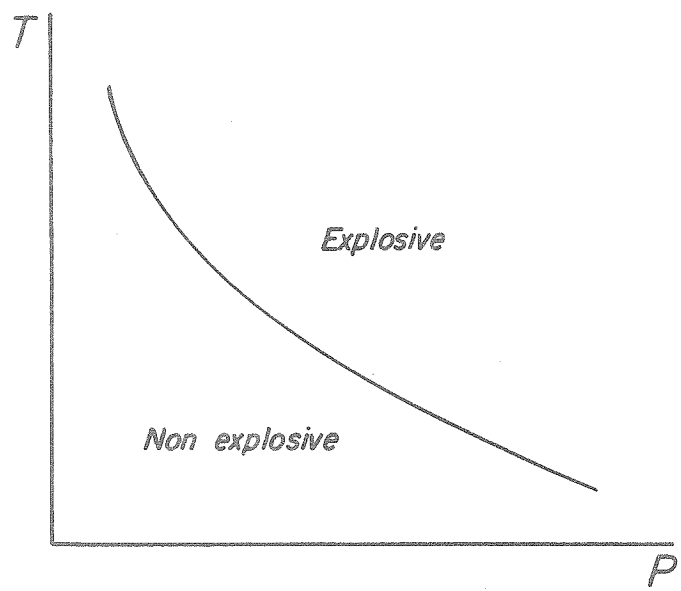

FIGURE 2

Typical explosion limit for thermal reaction

Later, the cause of the anomalous effects was found to be due to a branching chain reaction (6 to 11).

The reaction velocity for a chain reaction cannot in general be described by a simple relation depending upon the primary reactants only. This conclusion is due to the fact that the primary reactants do not combine directly, but an "active particle" is required to initiate the chemical combination. Many intermediate reactions may be present in the conversion of the reactants to the end products.

An example of a simple chain reaction is that of hydrogen and bromine. Here it is assumed that the chain carriers are the hydrogen and bromine atoms; thus,

$$H + Br_2 = HBr + Br$$

$$Br + H_2 = HBr + H$$

etc.

In this reaction, only one chain carrier is produced in each reaction, and the chemical combination will continue until the chain is broken or the reactants are consumed.

In the case of the oxygen and hydrogen reaction, more chain carriers are produced during a "reaction cycle" than are required to initiate the reaction. For example, consider the branching mechanism of the hydrogen-oxygen reaction; the hydrogen atom is assumed to be the active particle. (See Discussion of Results.)

$$H + O_2 = OH + O$$

$$O + H_2 = OH + H$$

$$OH + H_2 = H_2O + H$$

$$OH + H_2 = H_2O + H$$

Thus, three hydrogen atoms are produced for every one entering the cycle, and the reaction velocity would become infinite in a very short time if the chains were not broken by other reactions. This type of reaction is called a branching chain reaction. The set of chemical equations which consists of the actual branching and breaking reactions is called the "reaction mechanism".

It should be noted that the failure of the thermal theory to describe these more complex reactions does not mean that the rate equation is incorrect. It merely means that the law is not correctly applied to the reaction scheme. It is also interesting to note that there are several reactions of gaseous mixtures which do follow the simple thermal theory (12, 13).

In most cases, the formal laws of kinetics do not suffice to select with certainty the exact set of reaction equations. These various reactions are deduced by determining the intermediate products from spectroscopic or photochemical investigations.

A good example of a reaction mechanism for a branched chain reaction is that of hydrogen and oxygen. This reaction has been investigated quite thoroughly in the last thirty years. (For a survey, see reference 14, pages 315-325.) These investigations have determined fourteen probable intermediate reactions.

Von Elbe and Lewis (15) have solved a reaction mechanism for the case of the homogeneous reaction of a stoichiometric mixture ratio of hydrogen and oxygen in a constant volume spherical bomb. The reaction mechanism which Von Elbe and Lewis use is listed on the following page.

Three of the fourteen possible reactions are eliminated because their contribution to the process is doubtful. The number listed with each reaction is the number customarily used in literature to designate the reaction.

$H + O_2 = OH + O$	2
$OH + H_2 = H_2O + H$	1
$O + H_2 = OH + H$	3
$H + O_2 + M = HO_2 + M$ where M is a third body (H_2, O_2, H_2O)	6
$HO_2 + H_2O_2 = H_2O + O_2 + OH$	7
$HO_2 + H_2 = H_2O_2 + H$	11
HO_2 + (wall and adsorbed HO_2) = $O_2 + H_2O_2$	12
H_2O_2 + Dissociation = 2OH	i
H_2O_2 + Catalytic decomposition on wall = 2OH	13
$H_2O_2 + H + O_2 = H_2O + O_2 + OH$	5
$H_2 + O_2$ + wall catalysis = H_2O_2	14

These equations are solved by assuming that there is a steady reaction, and that each equation satisfies the rate equation independently. For example, the number of HO_2 molecules formed equals the number destroyed. The same condition is imposed upon the H and H_2O_2 particles. The relation for the number of H_2O molecules formed per unit volume per unit time is deduced, and the dependent terms in this equation are eliminated from the previous relations. The temperature dependence of the reaction rate coefficients for the various reactions are obtained from Arrhenius' equation (1). In

this way, an equation is obtained for the rate of water formation as a function of several constants which are determined from the experimental data. An excellent correlation between the theoretical and experimental work is obtained.

The inflections in the explosion limit curve (Fig. 1) are explained by Von Elbe and Lewis as follows. The shape of the first explosion limit is attributed to the adsorption of the active particles (H and HO_2) on the wall of the vessel. This process is possible because the mean free path of the molecules is larger if the pressure is lowered. As the pressure decreases, a larger percentage of the atoms and radicals reach the wall, where they are adsorbed. This limit is very difficult to determine experimentally because the rates depend very much upon wall effects. The second explosion limit is attributed to the gas phase destruction of the H atom by reaction 6, the mean free path being small enough to increase the probability of a three-body collision. The resulting HO_2 radical is then destroyed by wall adsorption. However, if the wall is not an effective adsorber, or if the pressure is increased further, decreasing the mean free path, the effective destruction of the HO_2 radical is reduced. Reaction 11 then becomes predominant, and an explosion results, giving the third explosion limit.

One serious handicap of the kinetic approach to combustion problems is the increasing complexity of the relations as more complicated fuels are considered. It is apparent, however, that this approach to the problem is the only one which can give

fundamental information.

An interesting aspect of the kinetic reaction scheme is the case where the explosion of a combustible mixture is apparently suppressed. For example, it has been known for many years that a wire can be placed in a combustible mixture and heated hundreds of degrees above the conventional explosion limit of the gas without causing an explosion. Similar phenomena have been noticed in petroleum refineries.

These results are hard to reconcile with the kinetic point of view, as in many cases explosions occur spontaneously in gases which are initially at room temperature. These explosions are attributed to a very rapid chain reaction following the admission of a few chain carriers. An example of this type of reaction is the ignition of hydrogen and iodine. A few intermediate particles are introduced by some mechanism (visible light in the case of the H_2 I_2 reaction) and the chain reaction takes over so rapidly that an explosion results almost instantaneously. In the hot wire experiments it seems evident that there must be a constant source of "active" particles. Thus it is difficult to see why the reaction does not initiate itself very rapidly.

Purpose of the Present Investigation.

The purpose of this research was to gain experimental evidence regarding the nature of a chemical reaction in the vicinity of a surface which is at a much higher temperature than the bulk of the explosive mixture.

The reason for investigating this particular case is based

primarily upon anomalous effects which have been observed in the oil industry. The safety codes governing the safe operating temperatures of heated surfaces which are exposed to combustible mixtures are determined by the following method. An open vessel is immersed in a lead bath and heated to the desired temperature. A predetermined amount of fuel (usually liquid) is introduced into the vessel and the explosion, or absence of explosion is observed. By varying the temperature of the vessel, the explosion limit and the safe operating temperatures of the fuel are determined.

In actual practice, it has been observed empirically that pipes and heated surfaces can be operated safely well above the temperatures specified by the safety code.

In view of these results and those obtained from the hot wire experiments, it appears that some phenomena are taking place which are not observed in the homogeneous reaction.

The reaction considered in this investigation is a great simplification of the problem as outlined. The simple reaction was chosen purposely because of the belief that an understanding of the mechanism in the simplest case is necessary before considering the complex reactions.

The experimental work in this thesis consists mainly of measurements of the temperature distributions in the explosive mixture. This particular measurement was chosen because of the belief that the determination of the temperature distribution in the explosive mixture would give direct evidence regarding the rate of heat

release, and some criterion regarding the propagation of the flame from the heated surface.

To obtain information regarding these mechanisms, an experimental arrangement was developed by Dr. Peter Kyropoulos and the author which could be used to impose a variable temperature gradient in the combustible mixture. The combustible mixture is contained in a shallow rectangular combustion chamber. This chamber is vented to the atmosphere so that a constant pressure reaction can be obtained. The temperature gradient is maintained in the gas by heating only one surface. The other is kept at a constant temperature. In order to obtain hydrodynamic stability of the combustible mixture, the upper surface of this chamber is heated. The temperature distribution between the two surfaces is measured with an optical interferometer. This instrument was chosen for two reasons. First, rapid changes in the temperature distribution were anticipated and an interferometer used with high-speed photography would be most suitable for these observations. Second, all disturbances due to temperature measuring devices are eliminated, and the inaccuracies in the temperature measurements caused by surface catalysis on thermocouple wires are removed.

The fuel tested was hydrogen and oxygen. These fuels were used for two reasons. First, the hydrogen-oxygen reaction is the simplest branching chain reaction, and second, there are good data available for the homogeneous reaction.

II. EQUIPMENT

The principal pieces of equipment which were used in this investigation may be tabulated as follows:

A. An optical interferometer of the Mach-Zehnder type (16, 17) was used to measure temperature distributions within the combustion chamber. This instrument, using interference phenomena, makes it possible to obtain these temperatures without placing instruments such as thermocouples within the combustion chamber. Thus disturbances due to surface catalysis and local effects of the instrument are eliminated. Figs. 3 and 4 show the interferometer frame and a closeup of one of the mirror supports.

B. A combustion chamber, shown in section in Fig. 6 was used to heat the mixture of hydrogen and oxygen. The chamber is made of two flat plates. The upper plate is provided with heaters and the lower plate is provided with cooling coils. Three variable transformers were used to control the temperatures and temperature distribution of the upper plate.

C. Electrically operated shutters (Figs. 7 and 8) were used to cover windows in the combustion chamber walls. These shutters were opened and closed electrically when the interferograms were taken.

D. A modified General Electric type AH-4 low-pressure mercury vapor lamp was used as the light source. Monochromatic

light was obtained by isolating the mercury green line with a Wratten 77A filter. The light was collimated with a ten-inch focal length simple lens.

E. Chromel and alumel thermocouples, all made from the same spools of wire, were used to measure the upper plate temperature. An Iron-Constantan thermocouple was used to measure the temperature of the lower plate. The calibration of the chromel and alumel thermocouples was checked with standard calibrated thermocouple wire obtained from the Leeds and Northrup Company. The calibration of the Iron-Constantan thermocouple was checked at the temperature of boiling water. The location of these thermocouples is shown in Fig. 6.

F. An injection rake (Fig. 9) was used to introduce the hydrogen and oxygen into the combustion chamber. This rake is arranged so the two gases are brought together a short distance from the combustion chamber.

G. Visible float rotameters were used to meter the flow of hydrogen and oxygen.

H. Adjustable diaphragm pressure reducing regulators were used to lower the oxygen and hydrogen tank pressures to slightly above atmospheric pressure. These regulators were also used to regulate the flow through the rotameters.

I. A sixteen-millimeter moving picture camera (Fig. 11) was used for recording the interferograms. Eastman Kodak Linograph

Ortho film was used in the camera.

J. A Leeds and Northrup eight-channel high-speed recording potentiometer was used to record the upper plate temperature (Fig. 13).

K. A Leeds and Northrup continuous recording potentiometer was used to record the lower plate temperature.

A schematic diagram of the equipment arrangement is shown in Fig. 15 and photographs of the complete installation are shown in Figs. 3, 16, and 17. This equipment is described in detail in the following pages.

A. Interferometer.

The interferometer used for this work is of the Mach-Zehnder type. The instrument consists of four mirrors which are located on the corners of the interferometer frame as shown. Two of the mirrors are aluminized so that approximately fifty percent of the light is reflected and fifty percent is transmitted. These mirrors are mounted on diagonally opposed corners of the frame. The remaining two mirrors are aluminized so that all of the light is reflected and are mounted on the other two corners of the frame. This device "splits" one beam of light into two separate beams. One beam passes through undisturbed air and the other beam passes through the combustion chamber. When the two beams are recombined at the second half-aluminized mirror, the varying density of the gas in the combustion chamber causes phase differences in the two beams, thus producing interference fringes. (See Appendix I.)

The mirror supports (Figs. 4 and 5) are made of invar. Each mirror is held against three support points in its frame by three very soft springs. Each support point is placed directly opposite the corresponding spring to avoid any bending of the glass mirror. The mirror frame is held firmly against three adjusting screws A, B, and C. (See Figs. 4 and 12.) Small ball bearings are fitted into the ends of the adjusting screws and fit into sockets in the mirror frame, thus facilitating adjustment and minimizing lateral movement of the mirrors. Screw C (Fig. 4) is used only for the initial location of the mirrors relative to each other. Adjustment of the mirrors is accomplished by turning screws A and B. These two adjustments are not completely independent, but little difficulty was encountered because of this arrangement.

Adequate adjusting sensitivity is provided in the following way. The adjusting screws A and B have a very fine thread (98 threads/inch). In addition, worm gear sets provide a relative motion of 50/1 between the adjusting screws and the adjusting wheel (Fig. 5). One-tenth of one turn of the adjusting wheel translates the adjusting screw approximately 5000 $\mathring{A}$.

Each mirror support and adjusting mechanism is assembled and fastened to the interferometer frame as a unit (Fig. 5). Provision for adjusting the light path length within the square formed by the mirrors is attained by a parallelogram leaf spring arrangement on two of the mirror supports (Fig. 5). The spring base allows the mirror support as a whole to be translated parallel to

the light path without rotation of the mirror.

The interferometer frame is made of two-inch pipe welded together as shown in Fig. 3. The frame was fully annealed after welding and the mirror support pads were machined in one setup so that the surfaces of the pads would be coplanar. Cooling water is circulated thrcugh the frame, which is lagged with one-quarter-inch thick asbestos cloth. Dimensional changes due to thermal gradients caused by convection currents in the room are thus greatly reduced.

In order to eliminate transmission of building vibrations to the apparatus, it is placed on rubber shock mounts. These in turn rest on the concrete floor of a room at ground floor level. No trouble was encountered due to floor vibrations with this arrangement.

Since there was no provision for keeping the room at constant temperature, considerable care was taken to make the interferometer installation as insensitive to temperature changes as possible.

It was necessary to provide radiation shields between the combustion chamber and the interferometer frame to prevent heating of the frame and mirror supports. Each shield is made of two sheets of bright aluminum, one inch apart. The bottom of the rectangular duct formed by the radiation shields (Fig. 17) is closed with asbestos paper to reduce convection currents around the combustion chamber proper.

Distortion of the interference pattern due to air currents in the room is reduced by passing the light paths of the three

remaining legs of the interferometer through two-inch aluminum tubing.

B. Combustion Chamber.

The combustion chamber consists of two flat plates 12 inches by 12 inches in size which are spaced one-half inch apart. This spacing is kept constant by allowing the upper plate to rest directly on ceramic blocks inserted between the plates. The upper plate is 3/8 inches thick and made of type 347 stainless steel. Walls, one inch in height, are welded to the upper surface of the plate, thus forming a shallow rectangular box. The heating elements, described in detail later, are placed in the space formed by the walls and are surrounded by lead, which serves as a thermostatic bath. A transite asbestos board covers the lead bath and supports the heaters. Under operating conditions, the lead is molten and acts as a heat transfer medium, thus reducing thermal gradients. The lower surface of the upper plate is machined and carefully polished. It was originally planned to plate this surface with one of the precious metals. This plan was discarded for two reasons: first, because it is very difficult to plate stainless steel, and second, because the metals which will stand the required temperatures without oxidizing are nearly all good catalysts.

The lower plate is made of one-half-inch thick copper plate and is chromium plated. Two helical counterflow cooling coils are soldered to the lower surface.

Three sides of the space between the two plates are closed by an 0.015-inch thick mild steel wall. The wall between the two plates is

kept in place by matching slots which are milled into the surface of the plates. The slots in the upper plate are milled so that the wall can be driven tightly into the slots, making the joints gas tight without the use of sealing compounds. The matching slots in the bottom plate are milled 0.010 inch oversize to facilitate assembly of the unit and to accommodate the thermal expansion of the walls during heating. The joints between the walls and the bottom plate are sealed with an asbestos cement.

The fourth side of the combustion chamber is covered with a blowout panel. This precaution allows an escape path for the gases in the combustion chamber should they explode. Two types of blowout panels were used. The most satisfactory panel was made of 0.002-inch thick steel shim stock pierced with ten 1/32-inch holes to provide an outlet when a steady flow of combustible gas was passed through the combustion chamber. A blowout panel made up of three thicknesses of quartz cloth was also tried, but was found to be too porous, permitting the gases in the chamber to be quickly contaminated with air when the flow was shut off.

The combustion chamber unit is mounted in a separate frame by means of lugs which form an integral part of the plates. This frame in turn is located within the interferometer frame.

The light beam is passed through square openings in opposite sides of the combustion chamber wall. These openings are in the centers of the combustion chamber walls and are placed on the axis perpendicular to the gas flow. These openings are covered with

electrically operated shutters and are opened only when pictures are taken. The shutters are made of transite asbestos board and are held tightly to the edge of the combustion chamber by leaf springs (Fig. 7). The shutters slide in a grooved rail which is fastened to the cold plate.

Initially, metal shutters were tried but were found unsatisfactory because they caused convection currents within the combustion chamber. These metal shutters were fastened to a steel shutter block which in turn was fastened to the edge of the combustion chamber. To minimize heat transfer between the two plates, the shutter block was insulated from the combustion chamber with an asbestos gasket. However, it was found that the shutter block would assume a temperature intermediate between the temperatures of the two plates. This caused the hot gas in the combustion chamber to flow into the opening in the shutter block where it cooled and then fell toward the cold plate, thus setting up convection currents within the combustion chamber. These convection currents caused the interferograms to be distorted so as to indicate incorrect temperature distributions.

The transite shutters, having a high thermal resistivity, attain approximately the same temperature gradient as the explosive mixture and thus minimize convection currents within the apparatus. The shutters are opened and closed by separate solenoids. The opening levers actuate microswitches as the opening solenoids bottom (Fig. 7). These microswitches are connected in series, and when both are

depressed, actuate a double relay switch which interrupts the current in the opening solenoids and closes the circuit for the closing solenoids (Fig. 18). As a result, one signal from the operator causes the shutters to open and close in a predetermined sequence. The shutters remain open for approximately 1/25th second, a feature which minimizes air contamination of the mixture in the combustion chamber.

C. Heating Equipment.

The upper plate of the combustion chamber is heated with eight stainless steel sheathed heating elements. The heaters are connected to three separate 230-volt variable transformers in such a manner that the four center heaters are supplied by one transformer, the second heaters in from each end of the hot plate are supplied by the second transformer, and the heaters on each end of the plate are supplied by the third variable transformer (Fig. 6). In this manner, heat addition along the length of the plate can be controlled to maintain a uniform temperature along the light path. Each of the heaters has a rated capacity of 600 watts. The rated total capacity thus is 4.8 kilowatts. It was found that the heating elements could be operated at an input of 30 percent above rated power because the lead bath prevented excessive sheath temperatures. To accomplish this, the variable transformers were wired in such a way that an output voltage as high as 260 volts could be attained.

D. Metering Equipment.

Hydrogen and oxygen from steel cylinders are supplied to the

combustion chamber by means of an injection rake which is silver soldered into the metal wall opposite the blowout panel (Fig. 9). This rake is made up of eight separate injection nozzles, all fed from common manifolds. Separate manifolds are provided for the hydrogen and oxygen, and the injection nozzles are connected to these manifolds by 1/16-inch inside diameter tubes. The gases are brought together approximately one inch from the injection nozzles. The small inside diameter of the tube insures complete mixing before injection. The injection nozzles consist of 0.005-inch slots which are cut through the upper surface of the tube and are perpendicular to the long axis. The admitted gas is thus injected upward toward the hot plate. This prevents the cool mixture from flowing across the bottom of the combustion chamber and through the blowout panel without coming in contact with the hot plate. This method of mixing the gases eliminates the necessity of having a large quantity of combustible mixture premixed and thus reduces the danger of flame flashback in case of an explosion. The flow of hydrogen and oxygen is measured by means of visible float rotameters (Fig. 14) which were calibrated with a water-displacement gasometer.

An electrical solenoid shutoff valve is placed in each gas line. These solenoids are connected to a hand switch which must be depressed to keep the valves open. This safety feature permits the operator to stop the flow immediately in case of an explosion.

E. Light Source.

The light source consists of a mercury vapor lamp and the mercury

green line (5461 Å) is isolated with a filter. It was found that when the mercury vapor lamp was operated at full voltage, the quartz capsule containing the mercury became incandescent and emitted a large amount of red light which was not satisfactorily filtered. It was also found that when the bulb was operated at full voltage, it reached a temperature at which line broadening caused the fringes to become indistinct. This difficulty was eliminated as follows: First, the mercury vapor lamp was operated at a reduced voltage, and second, the mercury vapor lamp was modified by cutting two holes into the outer glass tube surrounding the capsule. Cooling air is then circulated through these holes.

F. Recording.

The interference patterns are recorded with a sixteen-millimeter motion picture camera which is modified to take a seven-inch focal length lens. The camera is operated at sixty frames per second. It was found empirically that the best pictures could be obtained when the focal plane of the lens was near the center of the combustion chamber.

Large density gradients normal to the light path are caused by the large temperature difference between the two plates. This density gradient causes the light to refract as it passes through the combustion chamber, and since the density decreases in the upward direction, the light beam is deflected downward. This effect distorts the interferogram and also makes it impossible to obtain an image of the cold plate. The amount of the picture which is cut off by refraction of the light depends upon the angle at which the light enters the

combustion chamber. The distortion of the interferogram is minimized and the maximum field is obtained if the light enters at a small positive angle. (See Appendix II.) The adjustments to obtain the proper entrance angles are made by adjusting the location of the pinhole relative to the collimating lens. The interferograms are recorded on Eastman Kodak Linograph Ortho Recording Film. This film is of medium speed, has high contrast, and has high sensitivity to green light. The individual interferograms are enlarged approximately fourteen times and printed on paper of high contrast. The line spacings are read from the enlargement with an X-ray diffraction film reader.

The upper plate temperatures are measured by eight thermocouples, six of which are placed along the light path. The chromel-alumel thermocouples are inserted into 1/8-inch, two-hole ceramic protection tubes. The wires are cemented into the tubes with a cement made of Magnesium Oxide and Water-Glass to prevent the molten lead from shorting the wires. The thermocouple units are placed into 1/4-inch holes bored into the top surface of the hot plate. These holes are bored so that the bead of the thermocouple is 0.015 inch from the lower surface of the hot plate. The thermocouples are held in place by the transite cover over the lead bath. The thermocouple readings are recorded with an eight-channel high-speed Leeds and Northrup recording potentiometer. The cold plate temperature is measured with an Iron-Constantan thermocouple inserted into a hole in the bottom surface of the cold plate and made and placed similarly to the holes in the hot plate. This temperature was recorded with a Leeds and Northrup continuous recording Micromax.

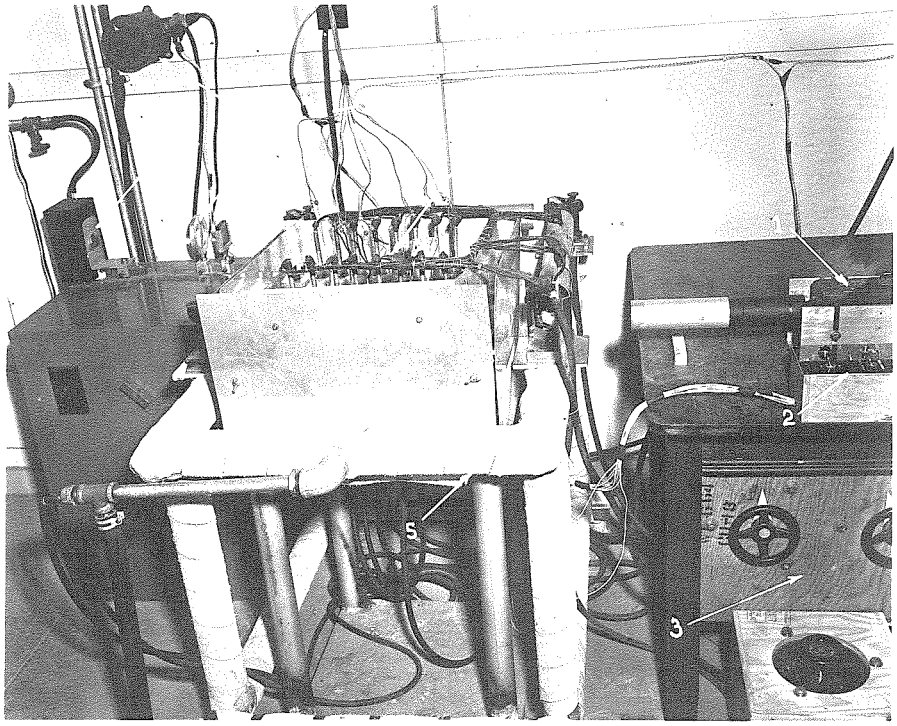

FIGURE 3. GENERAL VIEW OF EQUIPMENT

1. CAMERA
2. CAMERA AND SHUTTER CONTROL
3. VARIABLE TRANSFORMER CONTROLS
4. COMBUSTION CHAMBER ASSEMBLY
5. INTERFEROMETER FRAME
6. VARIABLE TRANSFORMER FOR LIGHT SOURCE
7. WRATTEN FILTER
8. COLLIMATING LENS
9. LIGHT SOURCE

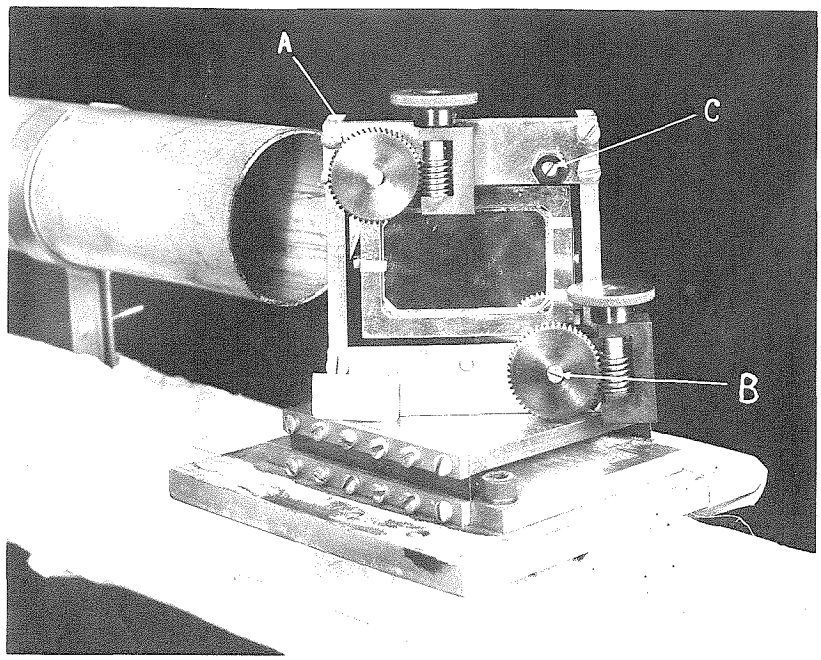

FIGURE 4. MIRROR ASSEMBLY
A,B,C, SUPPORT SCREWS FOR MIRROR FRAME

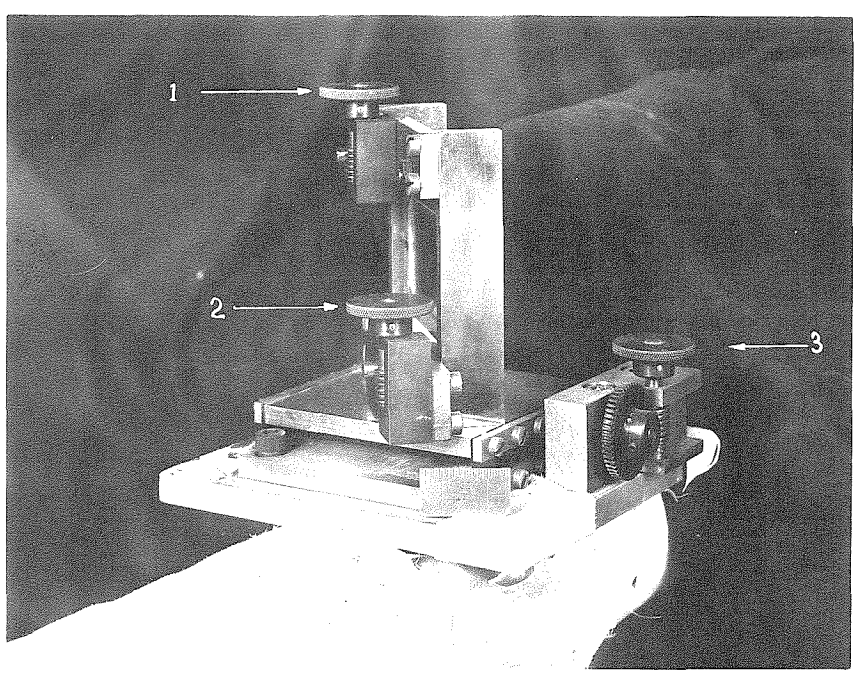

FIGURE 5. MIRROR ASSEMBLY
1,2 HANDLES FOR MIRROR ADJUSTMENT
3 HANDLE FOR LIGHT PATH ADJUSTMENT

FIGURE. 6

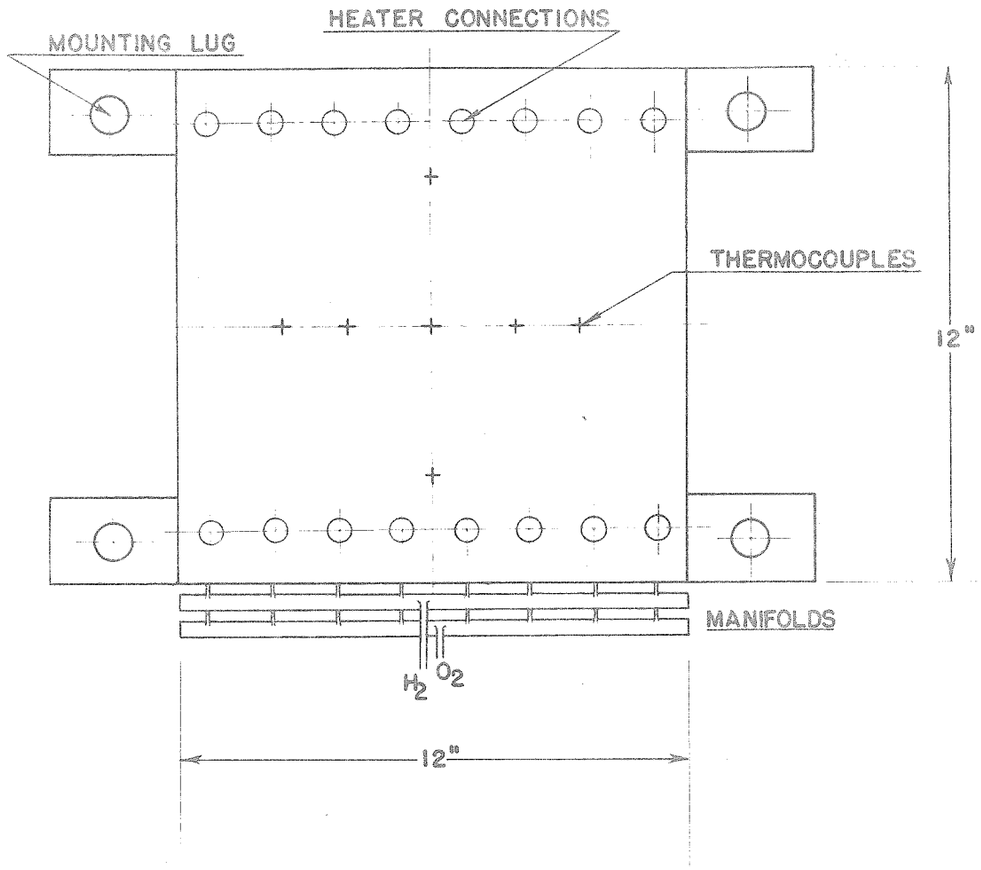

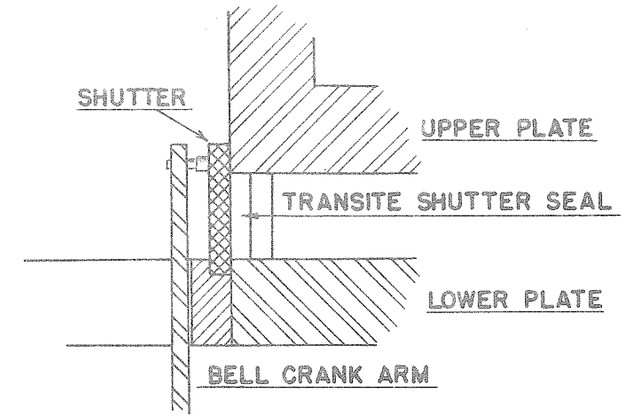

DETAIL A SHUTTER ASSEMBLY

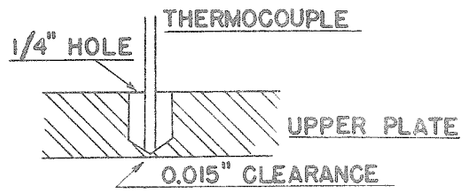

DETAIL B THERMOCOUPLE LOCATION

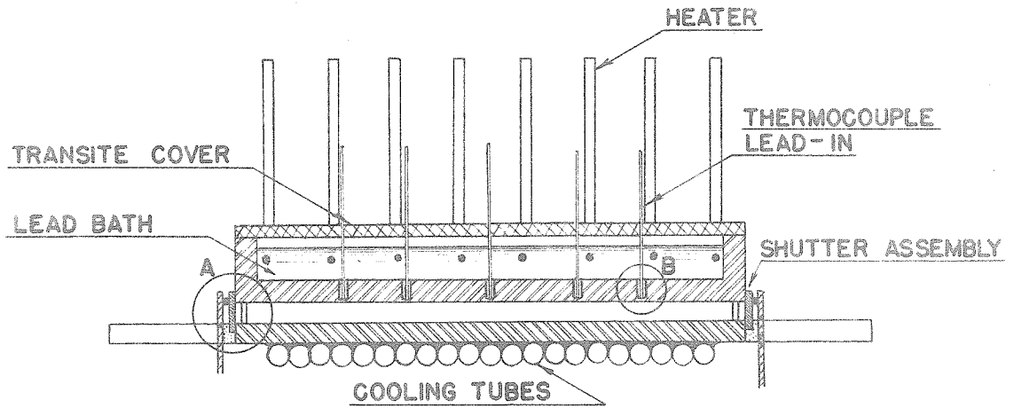

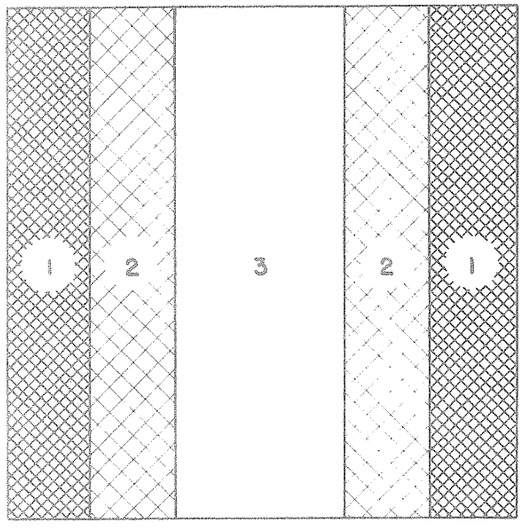

DETAIL C HEATER CONTROL DISPOSITION

FIGURE 6
COMBUSTION CHAMBER

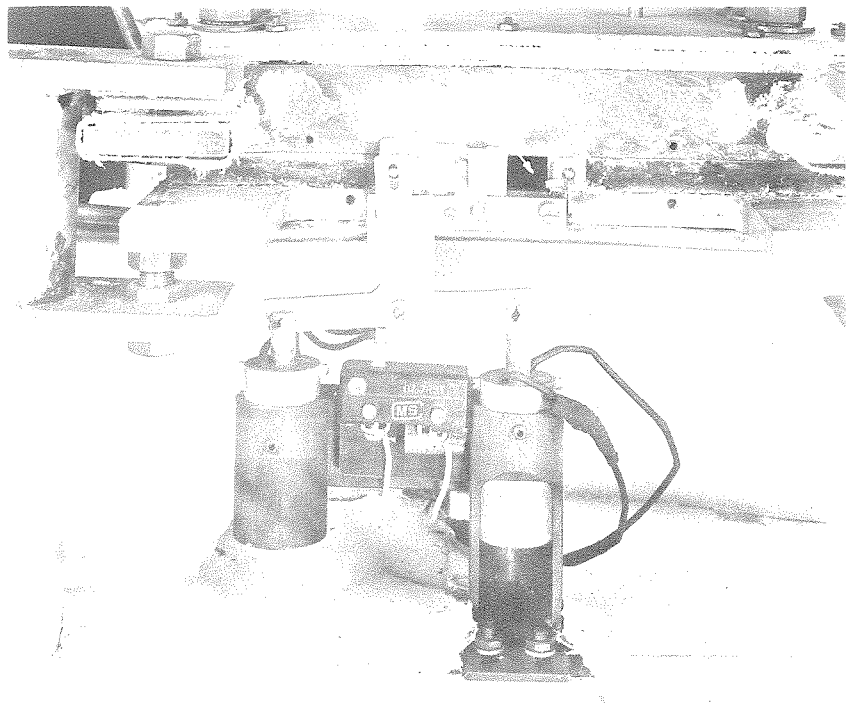

FIGURE 7. SHUTTER MECHANISM
1. TRANSITE SHUTTER
2. OPENING FOR LIGHT BEAM
3. LOWER PLATE

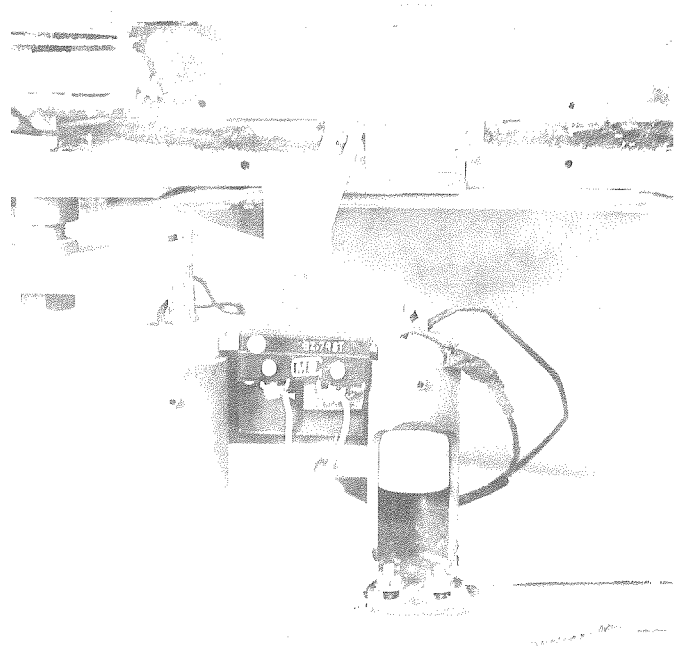

FIGURE 8. SHUTTER MECHANISM

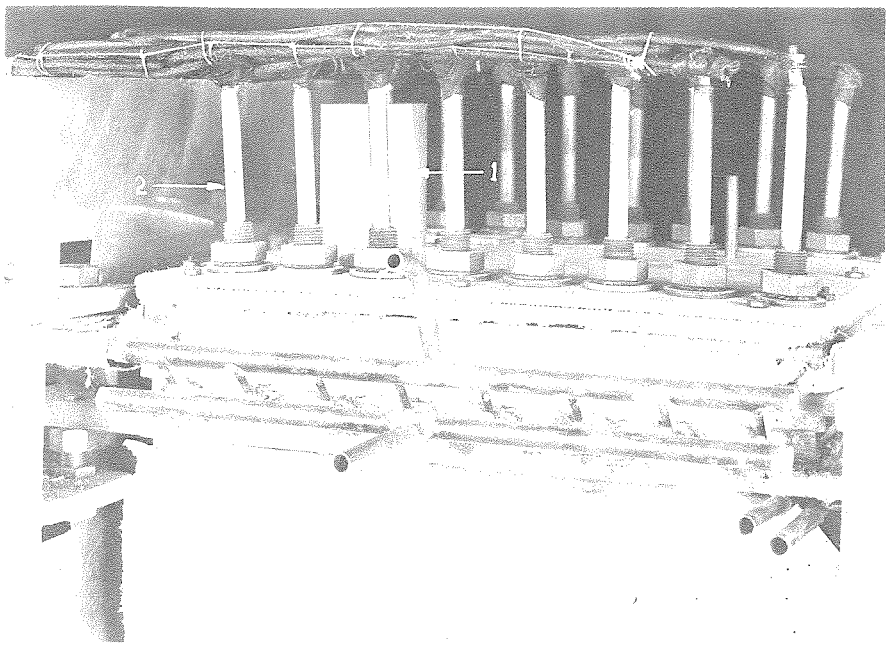

FIGURE 9. INJECTION RAKE

1. TRAP FOR LEAD VAPOR
2. HEATING ELEMENTS
3. HYDROGEN CONNECTION
4. OXYGEN CONNECTION
5. COOLING WATER CONNECTIONS

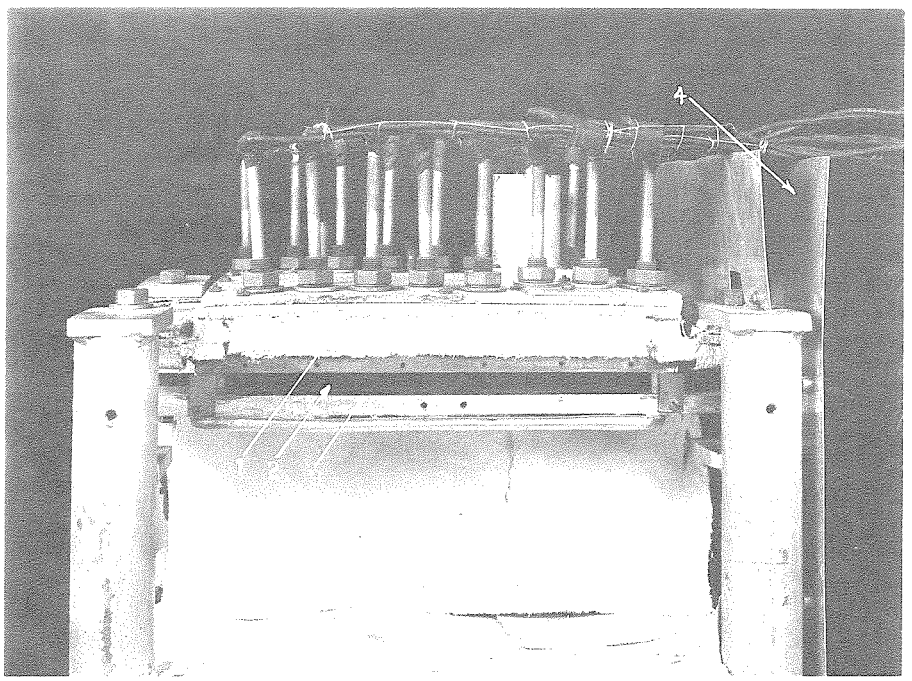

FIGURE 10. COMBUSTION CHAMBER ASSEMBLY

1. UPPER PLATE
2. OPENING COVERED BY BLOWOUT PANEL
3. LOWER PLATE
4. RADIATION SHIELD

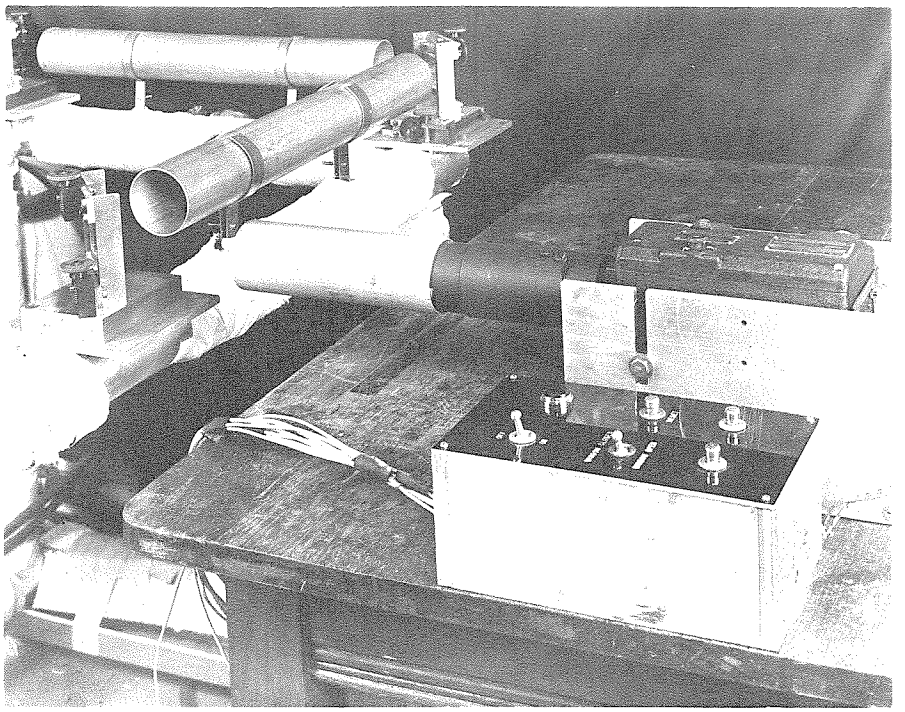

FIGURE 11. CAMERA AND CONTROLS

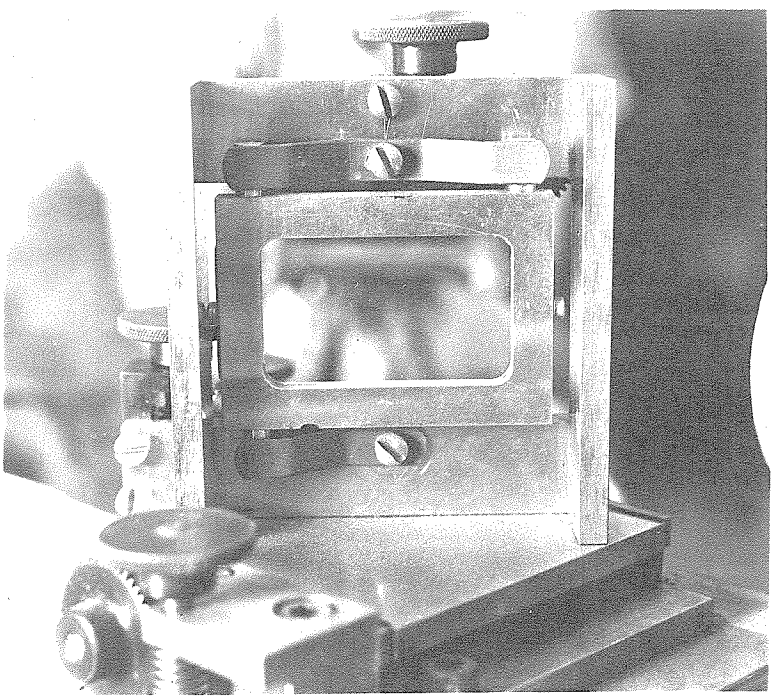

FIGURE 12. MIRROR FRAME AND SUPPORT

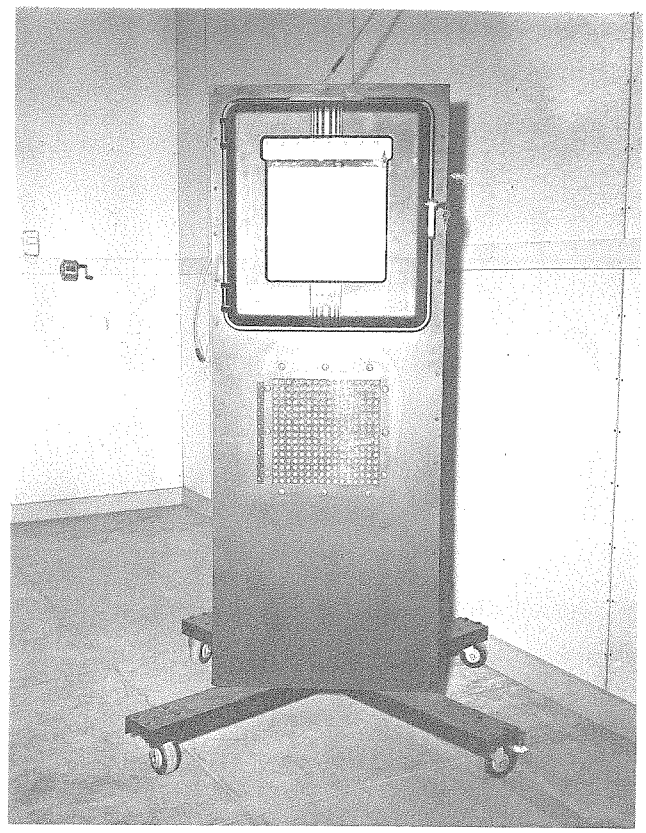

FIGURE 13. EIGHT CHANNEL RECORDING POTENTIOMETER

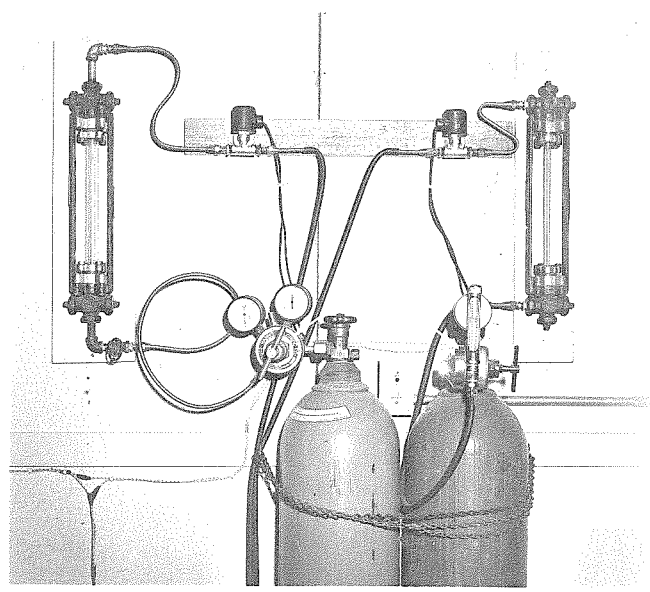

FIGURE 14. FUEL METERING EQUIPMENT
1. ELECTRICALLY OPERATED VALVES
2. OXYGEN FLOWMETER
3. HYDROGEN FLOWMETER
4. PRESSURE REGULATORS

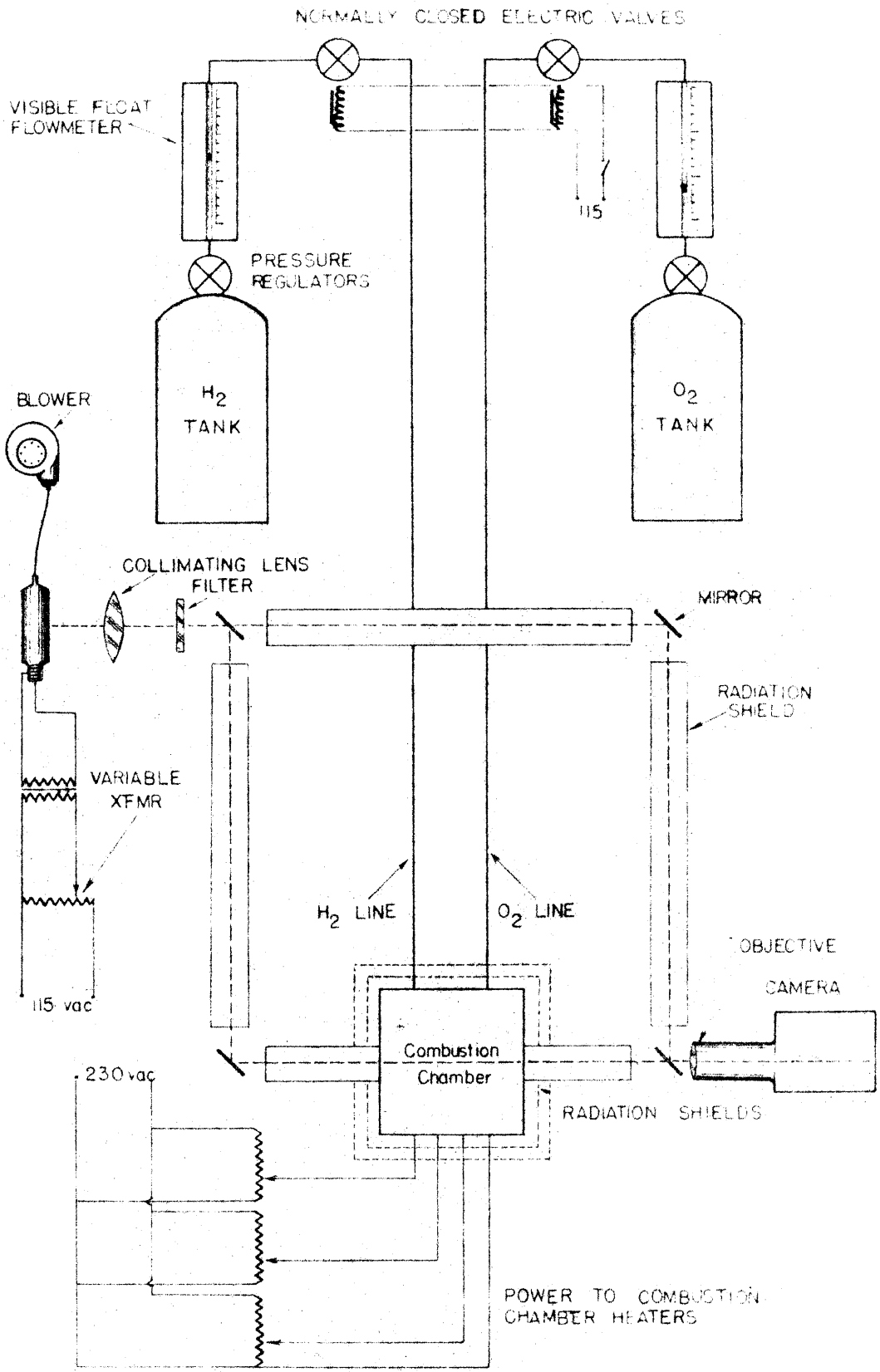

FIGURE 15. GENERAL SETUP

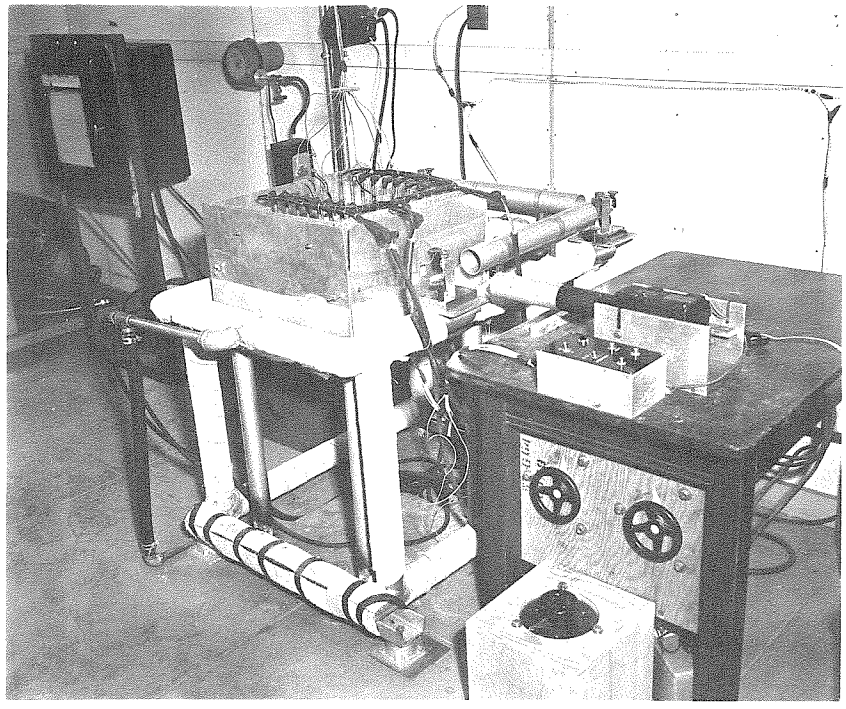

FIGURE 16. GENERAL VIEW OF EQUIPMENT

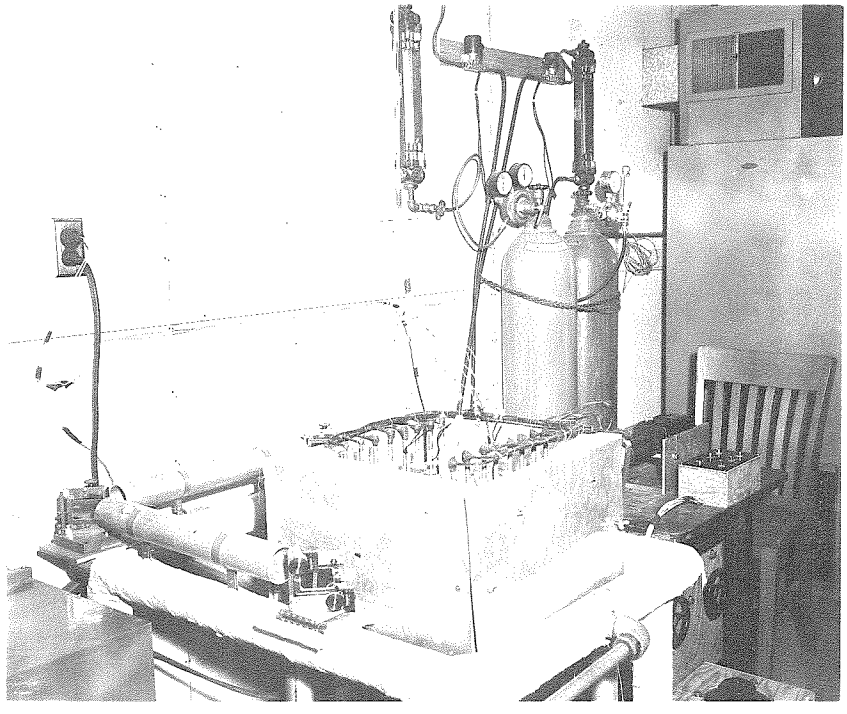

FIGURE 17. COMBUSTION CHAMBER AND INTERFEROMETER

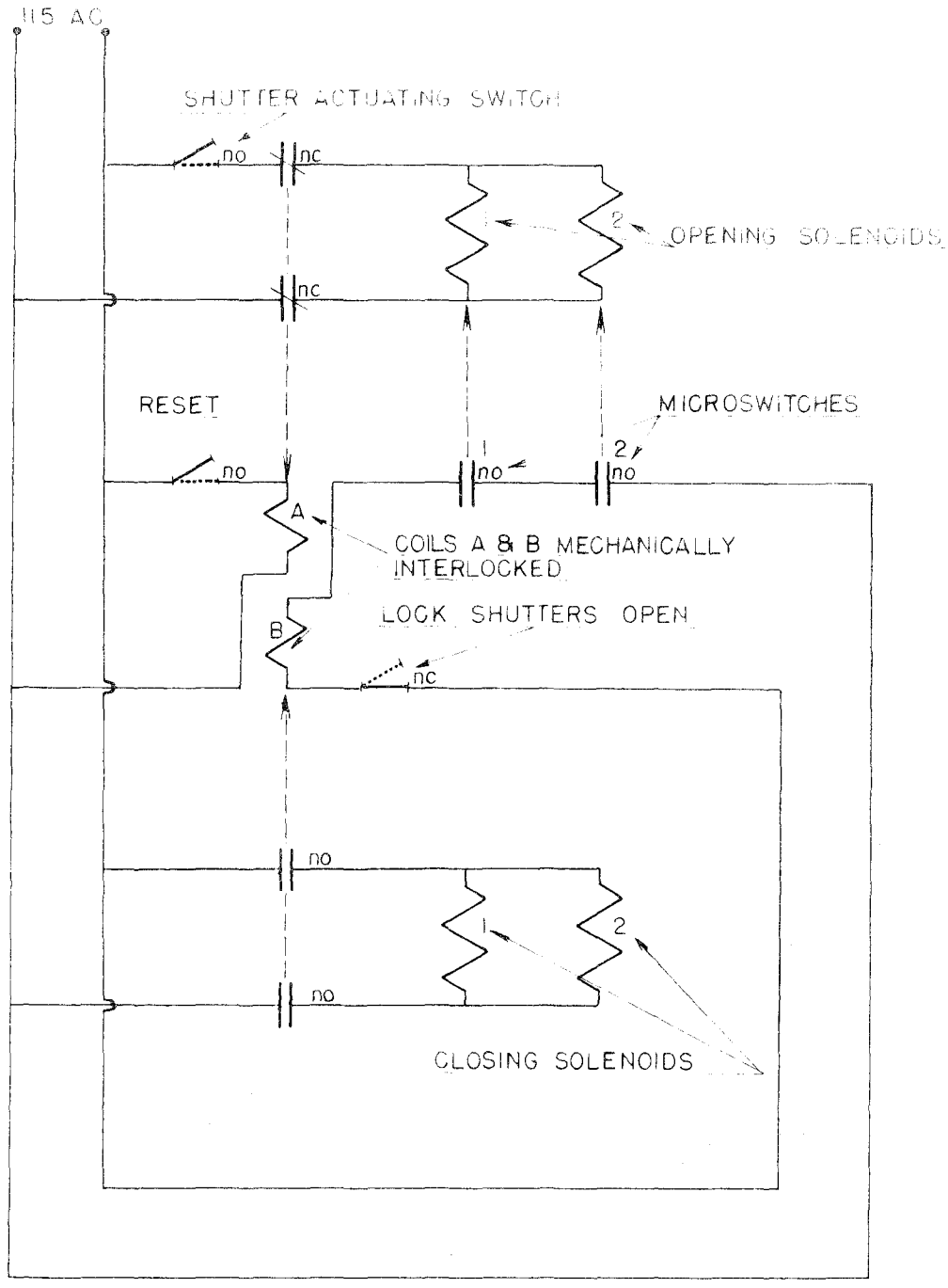

FIGURE 18. SHUTTER OPERATING CIRCUIT

III. METHOD OF ANALYSIS

Typical interferograms are shown in Figs. 22 and 23*. These interference pictures are reduced to temperature distributions in the following manner. The distance from the upper plate to each fringe is measured with an X-ray diffraction film reader. These distances are plotted against the fringe number on semi-log paper. A curve is faired through the points obtained at each temperature and the refraction correction (Appendix II) is subtracted from the ordinates of this experimental curve. The curve passing through the corrected points is then extrapolated to the cold plate, thus giving the number of fringes which would be observed in the absence of the refraction phenomena. The location of the lower plate on the enlargement is obtained from the enlargement ratio. This ratio is determined by placing a small steel cube in the combustion chamber which has two wires 0.010 inches in diameter inserted into holes in one face. The location of the wires relative to each other and the bottom of the cube are measured accurately. The block is placed in the combustion chamber so that an image of the two wires can be obtained on the negative. Thus, the enlargement ratio can be determined directly from the photographic enlargement.

The extrapolated curve is drawn to intersect the cold plate at an integral fringe number since the error in the extrapolation technique

*The "target" appearing in the interference pattern is caused by a reticule in the gun camera which was used for this investigation. The reticule was not removed as it was very useful for determining enlargement ratios.

does not warrant consideration of a fractional fringe number. The number of fringes found experimentally always exceeded the theoretical number by approximately two percent. This is attributed to end effects. A correction for the end effects is made by increasing the effective length of the light path by two percent. A temperature is then assigned to every fringe as described in Appendix I.

The accuracy of the temperature measurements is checked by comparing the experimental curve to a calculated temperature curve based on one-dimensional heat transfer. These comparisons were made for upper plate temperatures at which no appreciable reaction occurred. Since no experimental data are available for the thermal conductivity of a mixture of hydrogen and oxygen at these temperatures, it is assumed that the variation of the thermal conductivity with temperature predicted from the kinetic theory is correct (18). The constant in the heat transfer equation is evaluated at a known value of the thermal conductivity and temperature (19).

A great deal of trouble was encountered in securing good agreement between the calculated and measured temperature profiles. It was found that the original combustion chamber shutters were causing convection currents within the combustion chamber to such an extent that a large dip apparently existed in the temperature distribution near the upper plate (Fig. 21). The modified shutter which was described previously improved the correlation considerably (Fig. 21), but did not eliminate the anomalous effect entirely. It is possible that this effect is not due entirely to convection currents caused by the

shutters but is also a result of opening the shutters. Under operating conditions, the gas near the upper plate has a density about one-third that of the gas near the lower plate. Consequently, when the shutters are opened, convection currents start in a very short time. It was found empirically that the second picture on the film did not compare well with the first picture when the camera was operating at sixty frames per second.

Initially, quartz windows for the combustion chamber were considered. The excessive cost of quartz windows and the complication of the distortion of the interferogram due to the variation of the index of refraction of the windows with temperature were not justified at that time. It now appears that this modification would be advantageous.

It should be noted that the index of refraction of water vapor is about one and one-half that of the combustible mixture. Therefore, after the reaction has progressed an appreciable amount, the fringes near the upper surface appear closer together. When the temperatures are computed from the lower plate on the assumption that the gas is all hydrogen and oxygen, a marked change in slope of the calculated temperature is observed at the boundary of the two layers of gas. This effect can be observed only in the cases where the upper plate is a few degrees above the explosion limit. At higher temperatures, the reaction proceeds to such a degree that the water apparently diffuses throughout the gas, making it very difficult to determine the composition. An attempt to obtain an approximate curve was made by assuming

that only water existed at temperatures above the explosion limit. Temperatures are then computed from the upper plate. However, this assumption gives a temperature distribution profile which is not consistent with other considerations. (See Discussion of Experimental Results.)

Sample Calculation.

The interferogram shown in Fig. 22 represents a typical record from the data tabulated in Table I. The primary data for these records are as follows:

Measured upper plate temperature	1210° R
Measured lower plate temperature	551° R
Mixture ratio	Stoichiometric

The computation of the experimental temperature distribution for this upper plate temperature is as follows.

A plot of the fringe location as a function of the fringe number (measured from upper plate) is made on semi-log paper. This curve is shown in Fig. 24. To avoid confusion, only four of the six interferograms taken at this temperature are plotted. A curve is faired through the average of this group of experimental points as shown by the solid line. The refraction correction (Fig. 36) is subtracted from this curve, and the resulting corrected curve is shown in Fig. 24 by the dashed line.

The corrected curve is then extrapolated to the cold plate giving, in this case, 51 fringes. The theoretical number of fringes for these data is found from Fig. 30 to be 49.7.

If it is assumed that no reaction has taken place, the correction for end effects is

$$1 - \frac{N \text{ measured}}{N \text{ theoretical}} = 1 - \frac{51}{49.7} = 0.024 = 2.4\%$$

This value is typical of those obtained for upper plate temperatures lower than 1490° R.

The temperature distribution is computed from the cold plate by changing the direction in which the fringes are read. Thus the fringe number at the cold plate is zero. The temperature corresponding to each fringe is then read from a set of curves (similar to Fig. 30) which are corrected for end effects. These data are tabulated in the last two columns of Table I and the resulting temperature distribution curve is shown in Fig. 25.

The heat transfer curve in Fig. 25 is obtained as follows: For one-dimensional heat transfer, $Q = -k \frac{dT}{dy}$, and from the kinetic theory, $k \sim \sqrt{T} = D \sqrt{T}$. Combining these two expressions and integrating the resulting equation, the following relation is obtained.

$$Qy = - D \cdot \frac{2}{3} T^{3/2} + F$$

The value of k for a stoichiometric mixture of hydrogen and oxygen is found to be 0.0573 Btu/ft^2 hr °R/ft at 530° R. Evaluating D, and substituting its value into the integrated equation, the heat transfer equation becomes

$$Qy = - 1.659 \times 10^{-3} T^{3/2} + F.$$

The two constants in this equation are evaluated by using the

boundary conditions

$y = 0, \quad T = 551^{\circ}\ R$

$y = 1, \quad T = 1210^{\circ}\ R$

The final equation for y as a function of T is

$$y = 3.39 \times 10^{-4} \quad T^{3/2} - 4.39.$$

The solution is tabulated in Table II and is plotted in Fig. 25.

IV. ACCURACY OF MEASUREMENTS

In estimating the accuracy of the experimental data, the random and biased errors must be considered separately.

The biased error in the temperature distribution measurements may arise in several ways. For example, a consistent error in the mixture ratio of the reactants would cause a biased error in the temperature calculations. A bias could also result from the action of the combustion chamber shutters, or from consistent potentiometer errors.

It is difficult to estimate the magnitude of these errors. The biased error of the potentiometers is negligible as they were calibrated at several temperatures. The error in the fluid metering equipment is negligible also, as the rotameters were calibrated over their entire operating range. The biased error caused by the combustion chamber windows cannot be ascertained exactly, but an approximate value may be obtained by comparing the experimental temperature profiles with calculated profiles at low temperatures, 1210° R say. This error could be as large as five percent.

The other biased errors which should be considered are the variation of the temperature along the light path and the error in setting the location of the pinhole relative to the collimating lens. It was possible to keep the temperature constant to ± 3° R for approximately eighty percent of the light path. The temperature fell approximately 10 to 15° R (depending upon the absolute temperature of the plate) in the ten percent of the light path at each end of the

combustion chamber. The error in fringe number resulting from this temperature variation is approximately 0.2 percent and is negligible in comparison with the random error.

The estimated error in pinhole location is ± 0.005 inches. This causes an error of approximately plus or minus one fringe in the total number of fringes obtained.

The random errors are estimated to be:

Recording potentiometers	1½% of scale reading
Flow meters	2%
Extrapolation of interference pattern	1 fringe
Variation of interference pattern caused by convection currents	1 fringe

The total estimated error in the temperature distribution curves based on fifteen runs taken at various hot plate temperatures below the ignition temperature is estimated to be ± 4 percent of the temperature in degrees Rankine.

V. TEST PROCEDURE

The tests were conducted in the following manner: The interferometer frame cooling water was turned on and approximately ten minutes were allowed for the frame to come to thermal equilibrium. In the meantime, the mercury vapor lamp was turned on, allowed to warm up, and the combustion chamber windows were opened. After the interferometer frame had reached a constant temperature, the interferometer was adjusted so that the mirrors were parallel. (See Appendix III.) Then the cold plate cooling water flow was started and the power to the heating elements was turned on. During the time required for the combustion chamber to heat, the potentiometers were started and standardized. After the lead had melted in the thermostatic bath, the thermocouples were inserted into the upper plate. The variable transformers were then adjusted to obtain the desired temperature. After a uniform temperature distribution was obtained along the length of the upper plate, the oxygen flow was started; the hydrogen was then adjusted to obtain the desired mixture ratio. Approximately five minutes were allowed to flush the air from the combustion chamber. Then the gas flow was shut off by means of the electrical solenoid valves in the gas lines. The camera was started and allowed to reach full speed and the interferogram was taken by making electrical contact in the shutter circuit. A series of pictures was taken at various time intervals after the flow was shut off. In this manner the progress of chemical combination within the combustion chamber could be observed. This procedure was repeated at various temperatures of the upper plate.

VI. EXPERIMENTAL RESULTS

Typical results of the experimental work are shown in Figs. 22 to 27 and in Tables I and II.

Figs. 22 and 23 are typical interferograms obtained at plate temperatures of 1210° R and 1531° R respectively. As shown by these figures, the interferograms, though readable, could have greater contrast. The low contrast is caused by very thin negatives. The negatives were underexposed purposely to reduce the time required to make the enlargements.

Fig. 19 is a typical interferogram which was taken before the combustion chamber shutters were modified. The discontinuity in the fringe spacing is easily detectable by comparing this interferogram to that shown in Fig. 20. The interferogram shown in Fig. 20 was taken after the shutters had been modified.

Fig. 21 shows a comparison of the temperature distributions which were calculated from Figs. 19 and 20. As shown, the modified combustion chamber shutter improved the temperature distribution measurement considerably.

Figs. 25 through 27 show the temperature distribution curves for upper plate temperatures to 1615° R. Each curve is an average of six interferograms which were taken at the same temperature. As shown, the experimental curves for plate temperatures above 1500° R rise to a value much too high. This is to be expected because there is little doubt that some water has formed.

The maximum temperature at which interferograms were taken was 1615° R. Data were not taken at higher temperatures because it was not possible to maintain a uniform temperature along the light path. However, the center of the upper plate was operated at temperatures as high as 1710° R (experimental limit) without an explosion taking place.

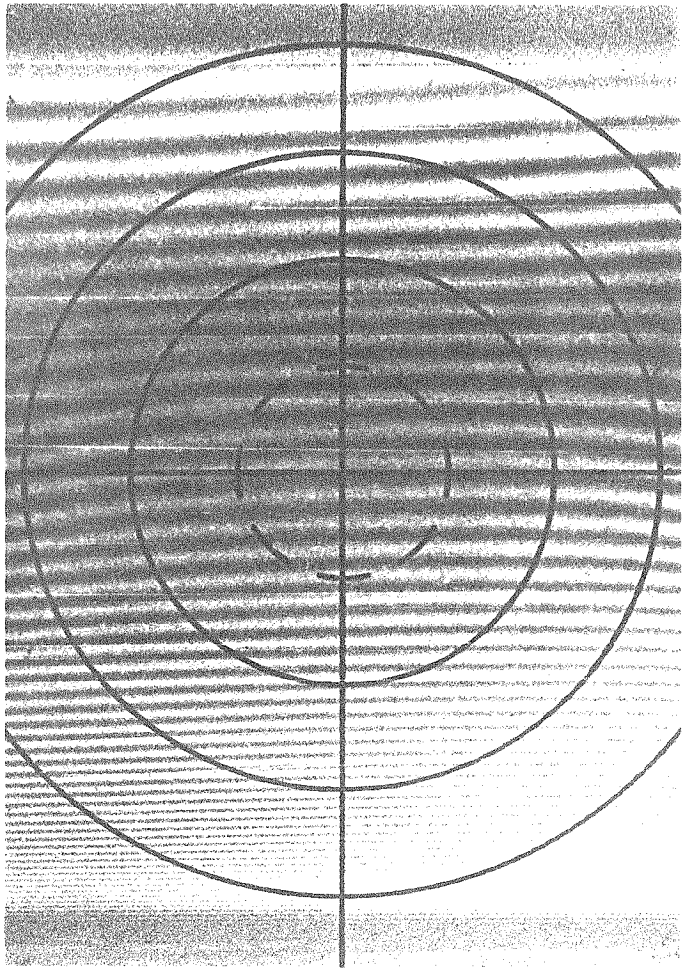

FIGURE 19. TYPICAL INTERFEROGRAM TAKEN WITH ORIGINAL SHUTTERS
TEST XIII-8 UPPER PLATE TEMPERATURE 1410° R

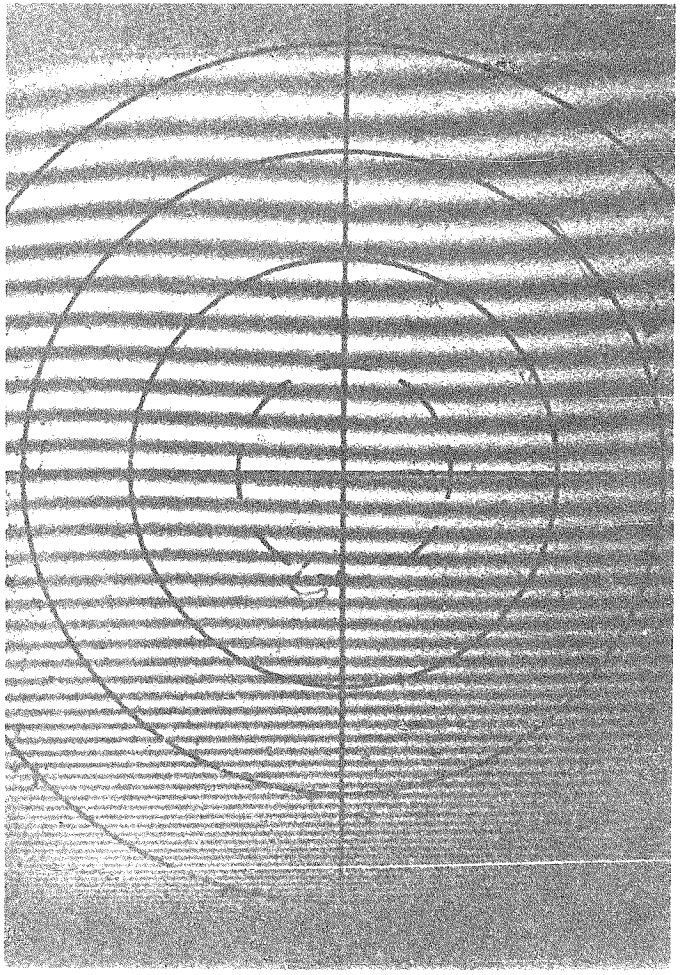

FIGURE 20. TYPICAL INTERFEROGRAM TAKEN WITH MODIFIED SHUTTERS
TEST XIX D-2 UPPER PLATE TEMPERATURE 1410° R

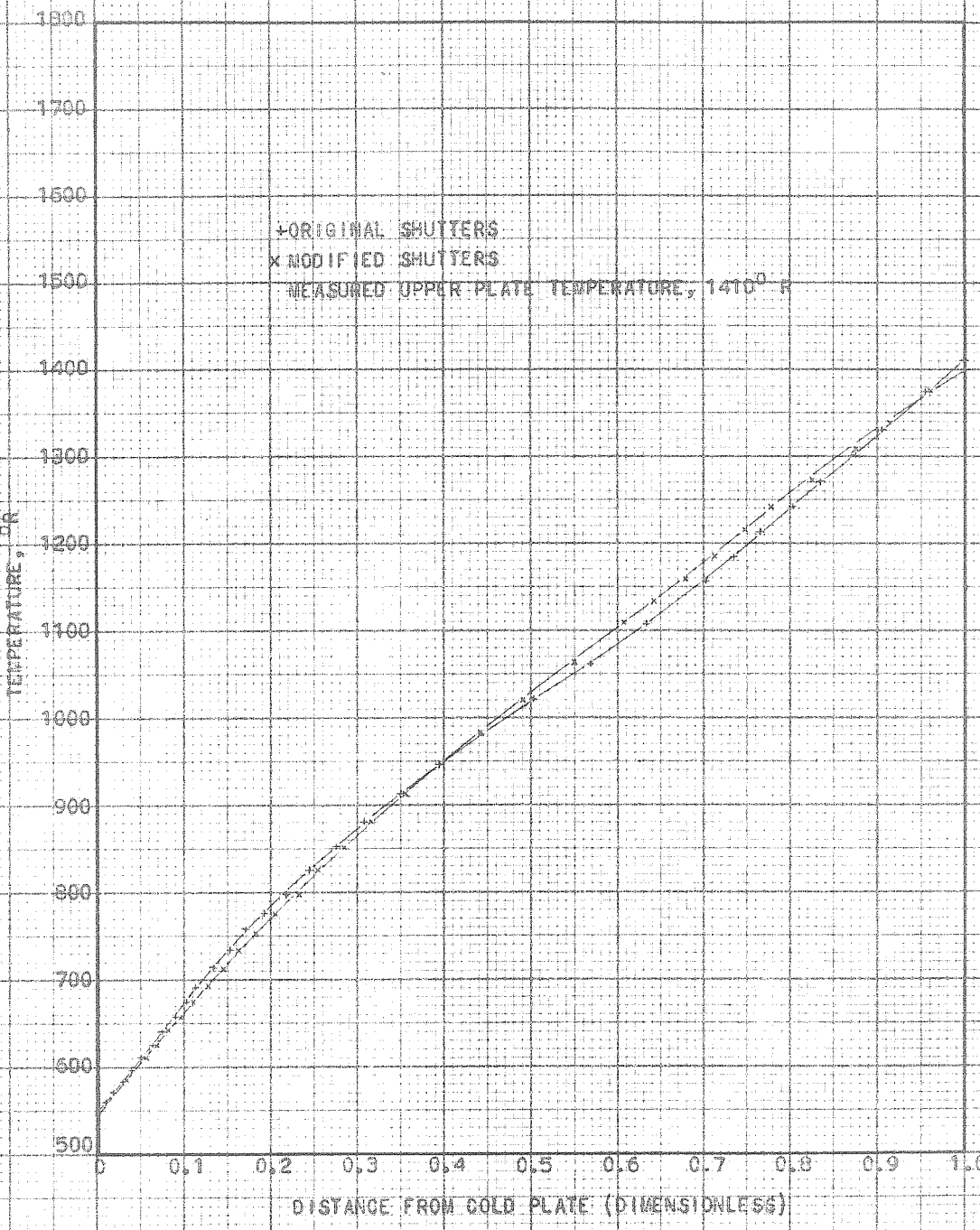

FIG. 21 EFFECT OF COMBUSTION CHAMBER SHUTTERS ON EXPERIMENTAL TEMPERATURE DISTRIBUTION.

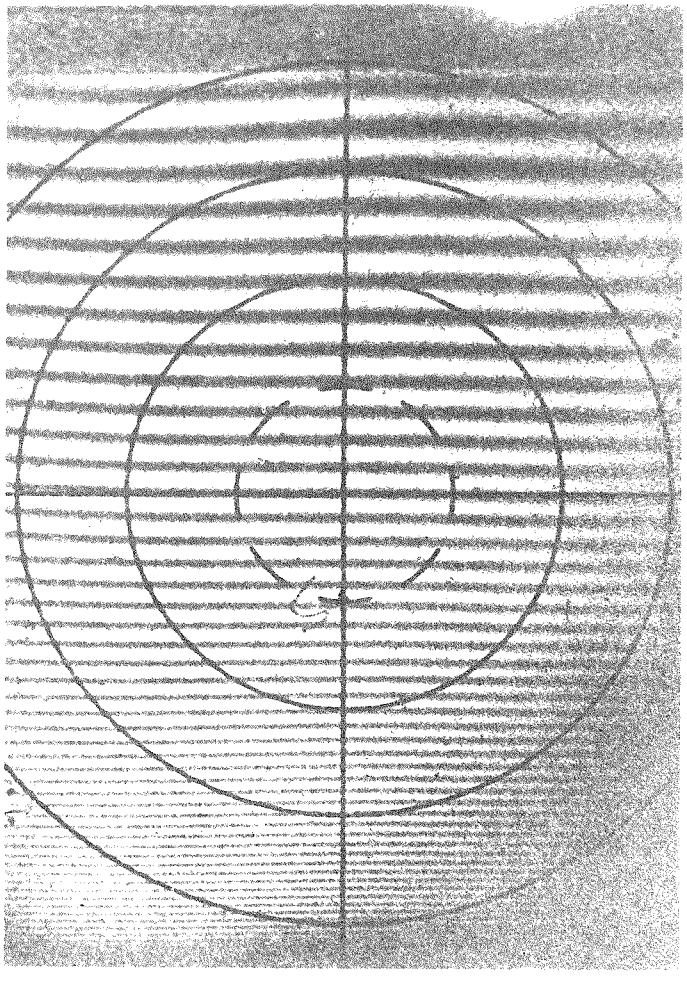

FIGURE 22. TYPICAL INTERFEROGRAM

TEST XX A-2 UPPER PLATE TEMPERATURE 1210° R

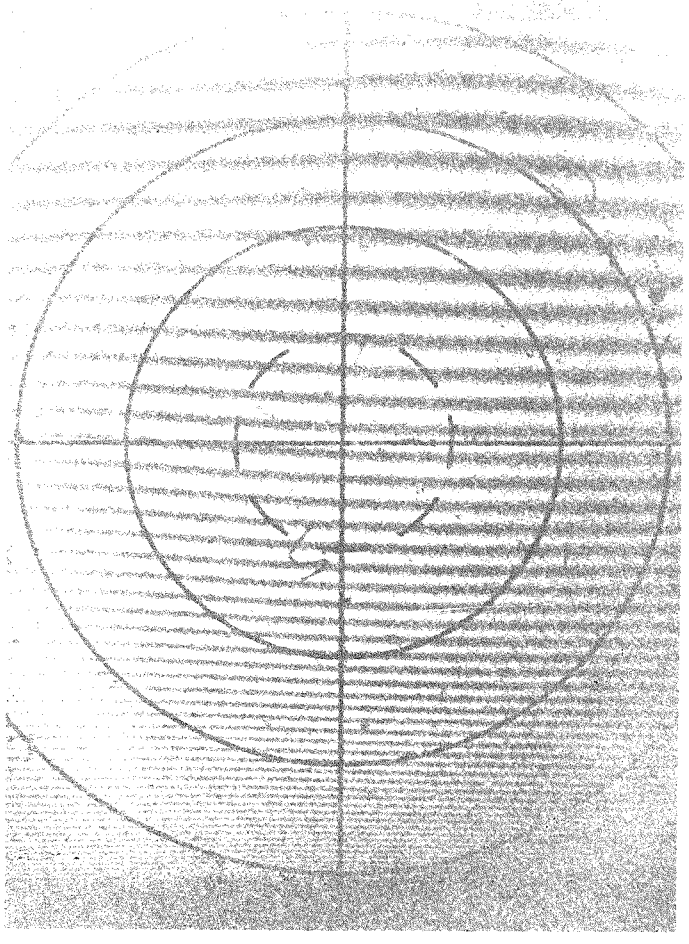

FIGURE 23. TYPICAL INTERFEROGRAM

TEST XIX N-1 UPPER PLATE TEMPERATURE 1431°R

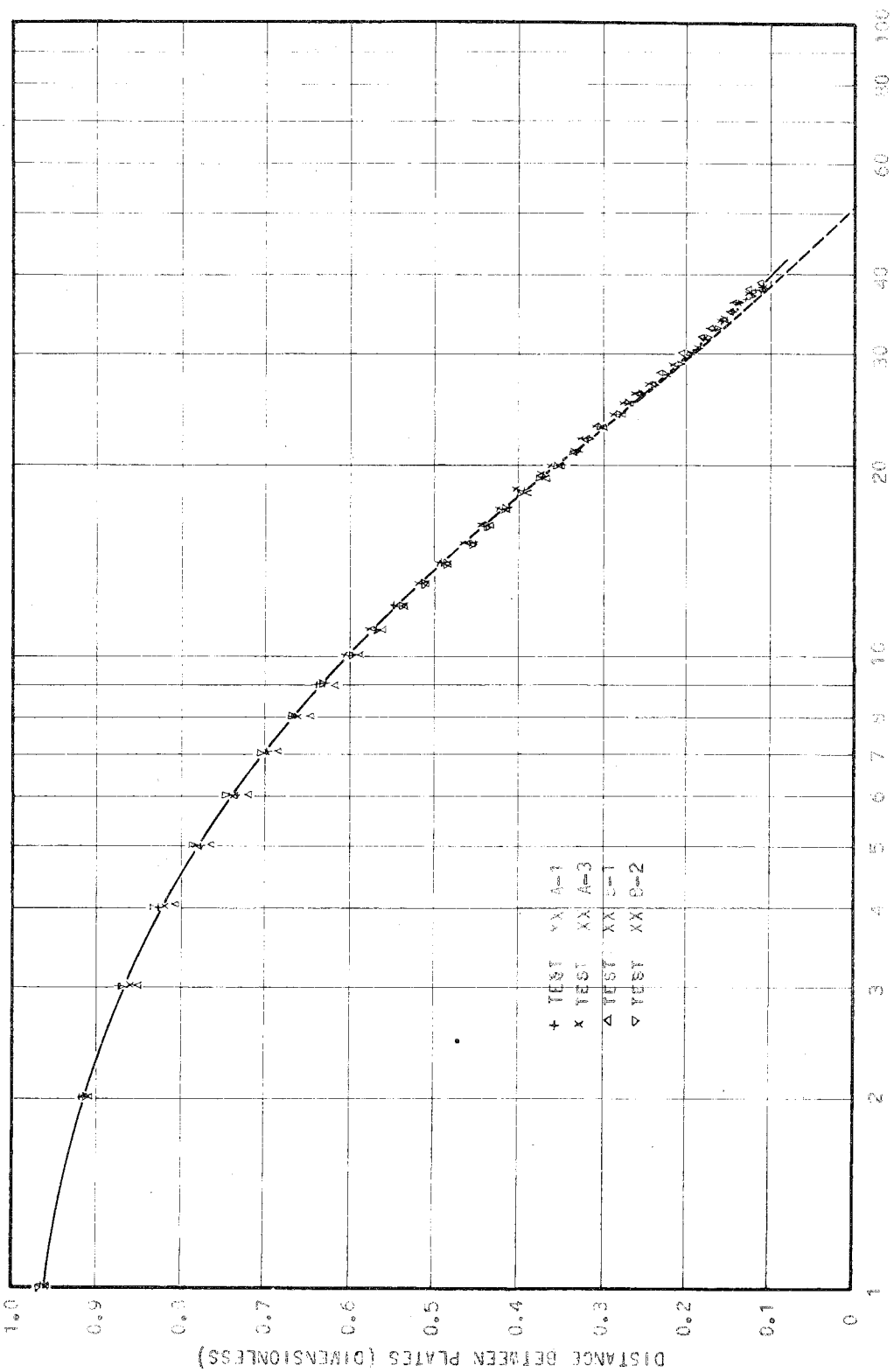

FIGURE 24. EXTRAPOLATION FOR TOTAL NUMBER OF FRINGES

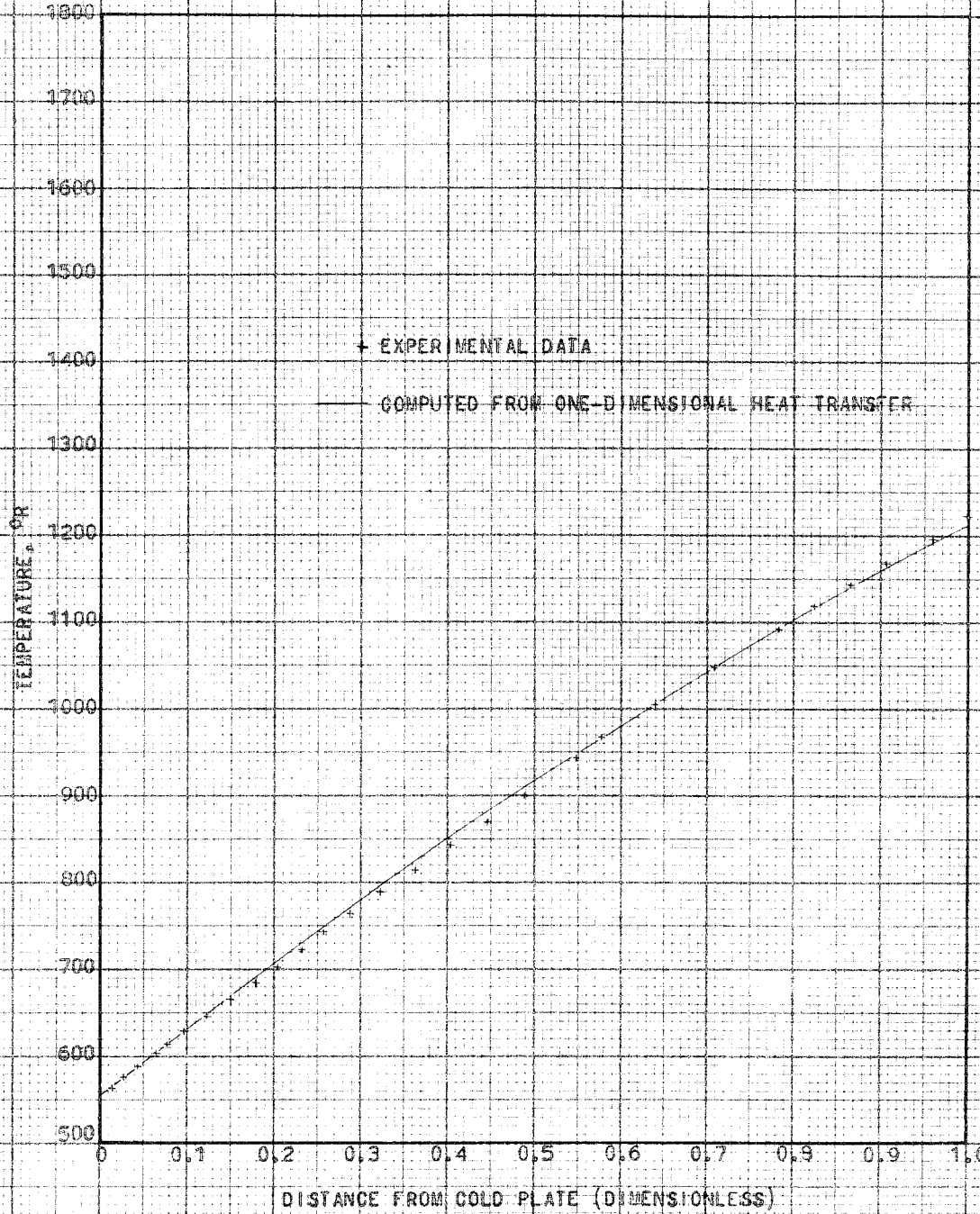

FIG. 25 COMPARISON OF EXPERIMENTAL AND THEORETICAL TEMPERATURE DISTRIBUTION CURVES.

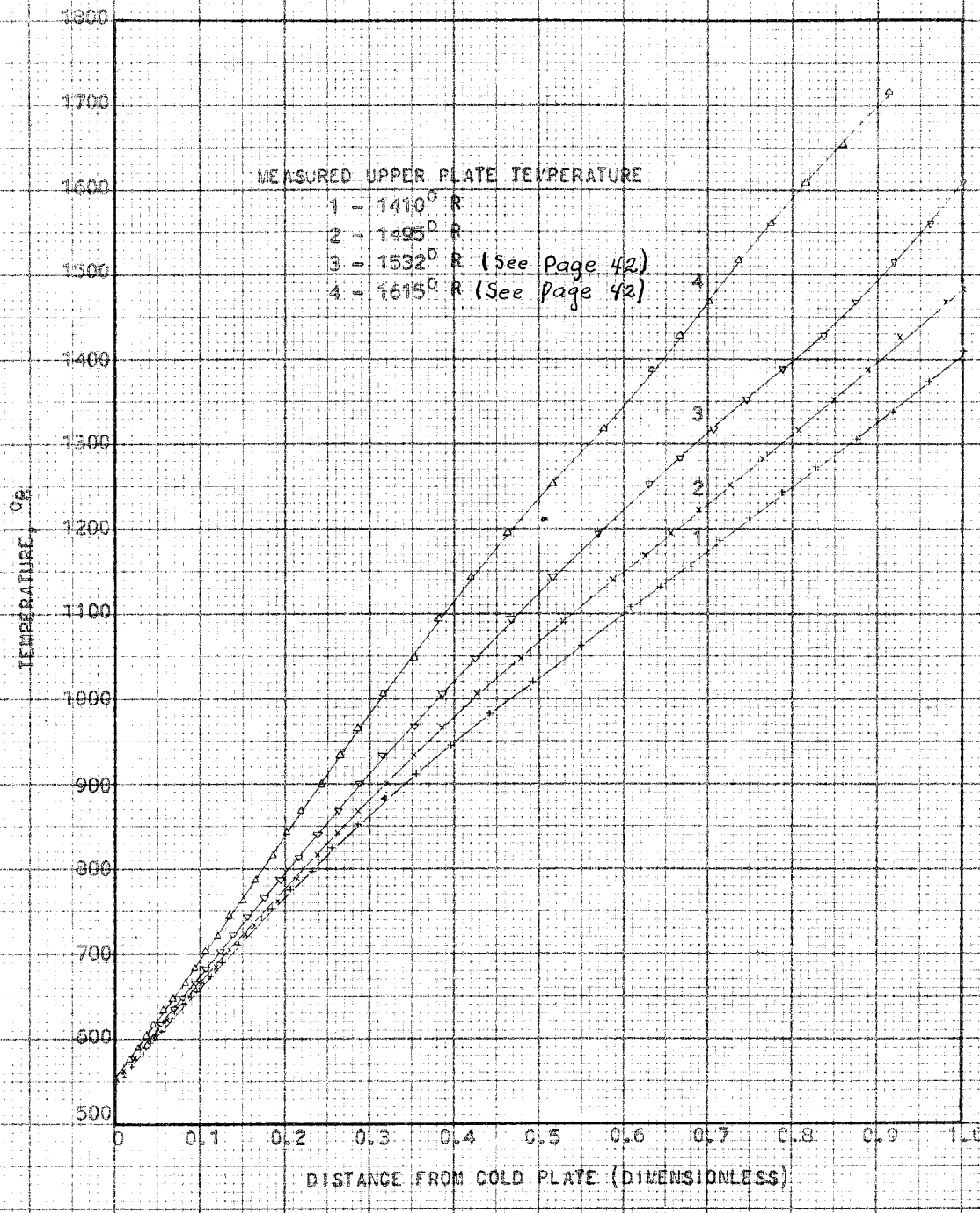

FIG. 26 EXPERIMENTAL TEMPERATURE DISTRIBUTIONS. ASSUMED GAS COMPOSITION $2H_2 + O_2$.

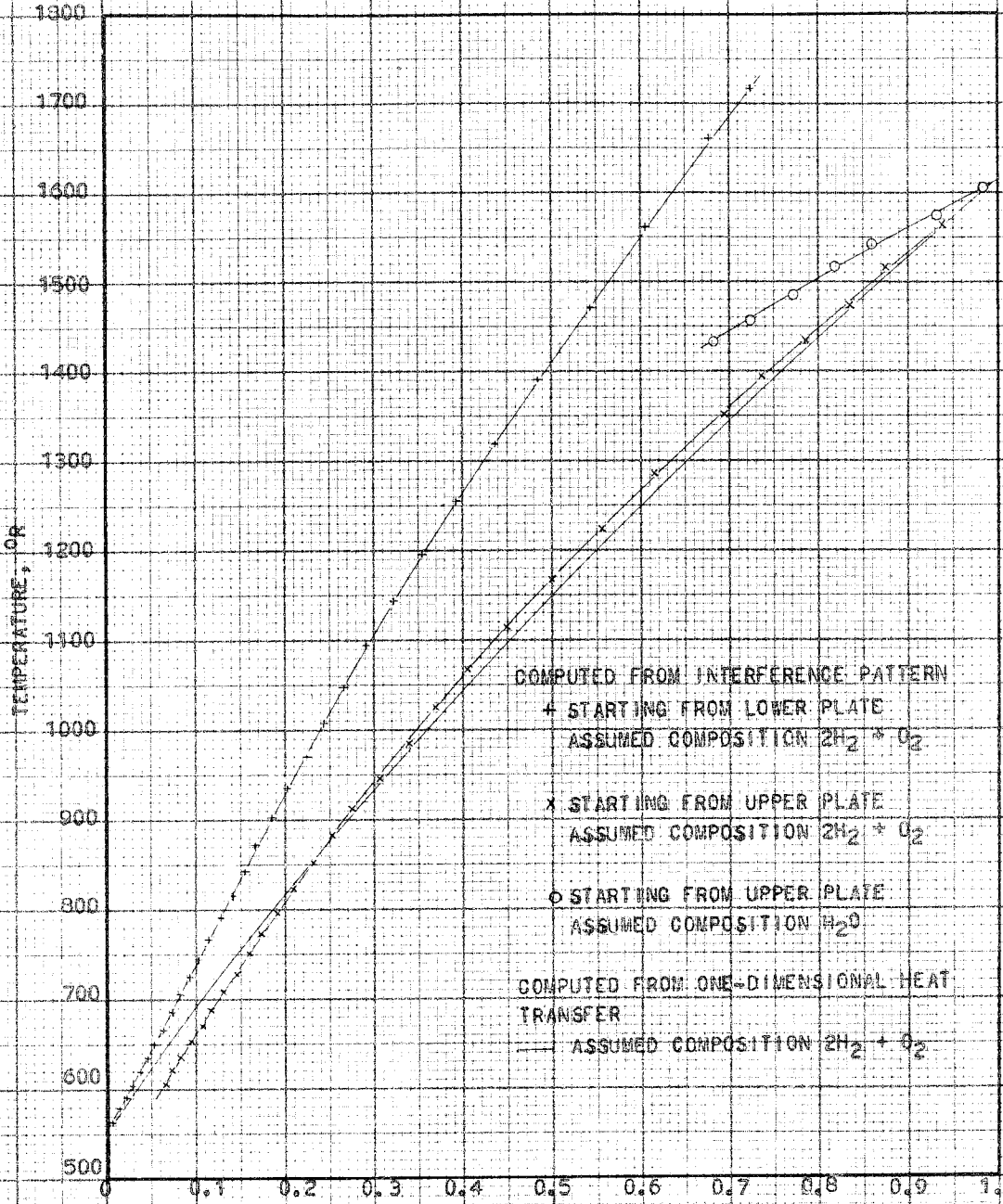

FIG. 27 COMPUTED GAS TEMPERATURE ASSUMING SEVERAL COMPOSITIONS.

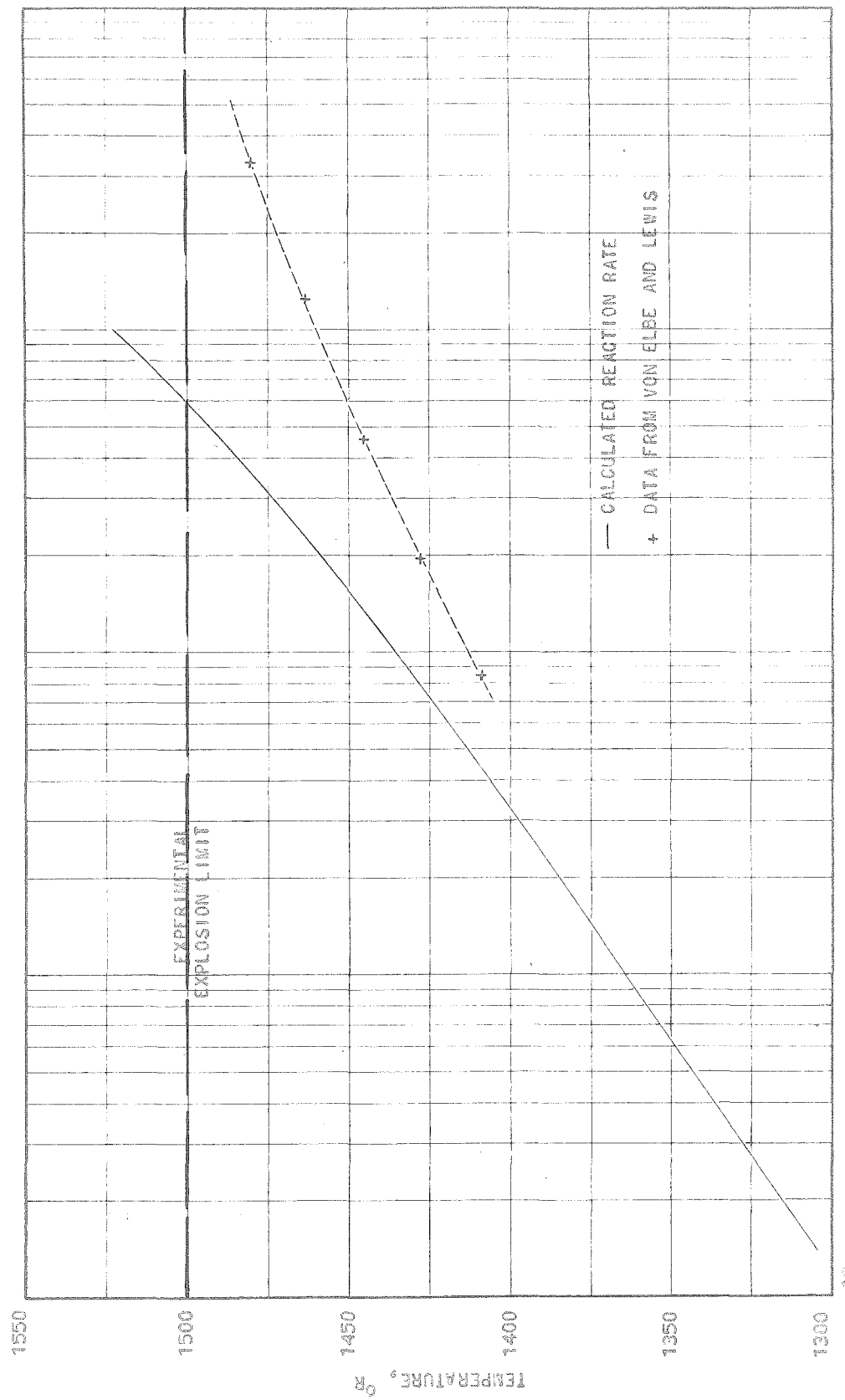

FIG. 20 COMPARISON OF THEORETICAL AND EXPERIMENTAL REACTION RATES.

TABLE I

TYPICAL INTERFEROGRAM MEASUREMENTS

FRINGE NUMBER FROM HOT PLATE	DISTANCE FROM HOT PLATE FRACTION OF PLATE SEPARATION TEST NUMBER				CORRECTED DATA FOR TEST SERIES XX A-B		
	XX A-1	XX A-3	XX B-1	XX B-2	FRINGE NUMBER	Y	T, ^{o}R
0	1.000	1.000	1.000	1.000	0	0	551
1	.950	.968	.953	.970	2	.014	563
2	.902	.908	.906	.920	4	.027	576
3	.857	.864	.903	.872	6	.045	589
4	.819	.824	.805	.833	8	.065	603
5	.777	.783	.761	.788	10	.077	618
6	.738	.744	.720	.746	12	.096	633
7	.706	.708	.682	.705	14	.120	649
8	.669	.672	.646	.668	16	.148	666
9	.639	.640	.613	.632	18	.178	683
10	.607	.608	.584	.599	20	.205	702
11	.578	.578	.559	.567	22	.232	722
12	.550	.548	.535	.535	24	.257	743
13	.528	.520	.509	.506	26	.288	765
14	.492	.497	.481	.482	28	.322	789
15	.467	.471	.458	.454	30	.363	814
16	.442	.447	.435	.432	32	.402	841
17	.418	.424	.413	.408	34	.445	869
18	.397	.402	.390	.388	36	.489	900
19	.376	.383	.368	.368	38	.548	983
20	.353	.365	.355	.348	40	.576	968
21	.337	.345	.333	.330	42	.640	1006
22	.316	.327	.316	.315	44	.707	1047
23	.299	.310	.301	.306	46	.782	1092
24	.282	.295	.287	.282	47	.824	1118
25	.266	.278	.274	.266	48	.865	1141
26	.251	.265	.258	.254	49	.908	1169
27	.237	.250	.245	.240	50	.958	1194
28	.222	.237	.232	.223	51	1.000	1222
29	.207	.221	.220	.209			
30	.195	.208	.206	.198			
31	.183	.196	.194	.184			
32	.172	.185	.183	.174			
33	.161	.175	.172	.170			
34	.151	.163	.156	.156			
35	.142	.154	.150	.145			
36	.132	.143	.142	.135			
37		.133	.130	.127			
38		.125	.124	.116			
39		.116	.115				
40		.107					
41		.097					

TABLE II

TABULATED DATA

THEORETICAL TEMPERATURE DISTRIBUTION

T	$T^{3/2}$	Y
551	1.293×10^4	0
600	1.470 "	.059
650	1.658 "	.123
700	1.853 "	.189
750	2.054 "	.257
800	2.262 "	.328
850	2.479 "	.401
900	2.700 "	.476
950	2.928 "	.555
1000	3.163 "	.633
1050	3.402 "	.714
1100	3.648 "	.798
1150	3.900 "	.883
1200	4.157 "	.970
1210	4.240 "	1.000

VII. DISCUSSION OF EXPERIMENTAL RESULTS

Experimental curves of the gas temperature versus a dimensionless distance between the two plates (the actual plate separation is 0.508 inches) for several upper plate temperatures are shown in Figs. 25 and 26. These curves are computed from the interference pattern on the assumption that the gas consists of hydrogen and oxygen.

Fig. 25 shows the experimental and the calculated temperature distribution for an upper plate temperature of 1210° R. At this temperature, it is assumed that the reaction rate is negligible. As shown, the experimental curve crosses the calculated curve near the center of the plate separation. It is assumed that the deviation of the experimental curve from the theoretical curve is caused by opening the combustion chamber windows. The effect appears on all of the records, and a temperature distribution of this type is not reasonable from heat transfer considerations. The thermal conductivity of the gas should not vary in such a manner. The assumption that no appreciable reaction is taking place seems justified on the basis of data obtained at higher temperatures, and upon a theoretical calculation of the reaction rate as a function of temperature. Curves 1 and 2 (Fig. 26) show similar distributionsfor upper plate temperatures of 1410 and 1495° R respectively.

It appears from the shape of these curves that no appreciable reaction is taking place until an upper plate temperature of 1500 ± 10° R is reached. This observation is justified on the basis of the following discussion.

A simplified calculation was made to obtain the theoretical reaction rate of the homogeneous reaction as a function of temperature. It is assumed that the hydrogen atom is the active particle which initiates the chemical combination. The rate of chemical combination is assumed to be governed by the equilibrium concentration from thermal dissociation of the hydrogen atom. This concentration is calculated from the free energy change (20). It is assumed that the reaction involving the hydrogen atom is slow enough that the equilibrium concentration of hydrogen atoms is disturbed very little.

The actual reaction rate is computed by determining the number of collisions per unit time per unit volume that the hydrogen atoms make with oxygen molecules. This number is multiplied by a "yield" factor. The yield factor is essentially the fraction of the total number of particles which have an energy equal to, or above, the activation energy required for the following reaction.

$$H + O_2 = OH + O \text{ (activation energy 14 Kcal/mol)}$$

Thus the reaction rate is given by the relation (28)

$$w = \frac{dH_2O}{dt} = N \frac{E_o}{RT} \cdot e^{-E_o/RT}$$

where w is the number of water molecules formed per unit volume per second, N is the number of impacts per unit volume per second, E_o is the activation energy, T is the absolute temperature, and R is the universal gas constant. The yield factor given above includes the vibrational energy of the molecule participating in the reaction as well as the translational energy of both particles.

The computed curve of the reaction rate is plotted as a function of temperature in Fig. 28. This curve is compared to a similar curve which is taken from Von Elbe and Lewis' data. As shown, the correlation is quite good. The fact that the experimental data show higher rates is probably due to chain branching. The higher experimental rates may also be due to high local temperatures caused by self-heating of the combustible mixture. This effect would cause a greater difference between the two curves as the explosion limit is approached. From this comparison, it appears evident that the hydrogen atom is the primary chain carrier. It is also evident from these curves that at upper plate temperatures below 1480° R, one would not expect to observe a change in the interference pattern during the nine seconds the mixture is under observation.

The fact that no detectable reaction occurs below a temperature of 1500° R is also a good indication that the catalytic reaction on the upper surface is very small. The validity of this conclusion is justified as follows.

Previous work (21) has shown that 1500° R is the temperature of the explosion limit at atmospheric pressure for a reaction taking place in the absence of a surface. These experiments were made with impinging jets of preheated gases. Von Elbe and Lewis also found 1500° R to be the explosion limit of a stoichiometric hydrogen-oxygen mixture at atmospheric pressure. Their experiments were conducted in salt-coated spherical vessels. The vessels were

coated with various salts to obtain a surface whose properties do not change during the reaction. The necessity of this technique is due to "poisoning" of the vessel surface with water vapor which apparently changes the surface properties. Thus, consecutive experiments are not reproducible.

No attempt was made to treat the surface of the upper plate with these salts because the results of the experiments were reproducible. The surface of this plate became covered with a thin film of chromic oxide which is apparently very stable.

It is not definite that a catalytic reaction did not take place in these experiments for two reasons. First, it is not possible to detect a very thin layer from the interferogram, and second, the reaction rates, say at 1480° R, are so slow that it would take approximately three or four minutes to produce enough water to be detectable. The period of observation in these experiments was limited to approximately ten seconds after the flow had been shut off. This limitation is due to the fact that air enters the combustion chamber through the escape holes in the blowout panel after the gas flow is shut off.

However, the gas which is in the combustion chamber has had approximately one minute to react before the pictures are taken. Therefore, if the reaction is progressing at an appreciable rate, it should be detectable from the interferogram, as the water should diffuse into the main body of gas and change the total number of fringes.

At plate temperatures above 1500° R and below 1540° R, an appreciable discontinuity in the calculated temperature profile is observed near the upper plate (Fig. 26, curve 3).

This discontinuity could be caused by the following mechanisms:

1. Heat is added in this region by the chemical reaction.
2. The water vapor in this region absorbs radiation from the upper plate.
3. The observed fringe spacing is caused by a variation in the composition of the gas mixture.

The first two effects cannot alter the shape of the temperature curve appreciably, as the heat added due to the reaction cannot be more than one-half of one percent of the heat transferred by conduction, and the radiation absorbed by the water cannot be more than five percent of the total heat transferred by conduction. This can be shown as follows. First, a simple heat transfer calculation predicts that approximately 0.7 Btu/ft^2 sec is conducted through the gas. The total amount of heat which the volume of combustible mixture can release is approximately five Btus. Thus to influence the shape of the heat transfer curve, it would be necessary for the reaction to be progressing at such a rate that the reactants would be consumed in approximately one minute. Second, an estimate of the quantity of heat absorbed by the gas can be obtained from charts presented by Hottel (22). The rate at which heat is being absorbed from a black emitter at 1560° R is computed for a rectangular slab of water vapor one-quarter of one inch thick and at atmospheric

pressure. Hottel's charts indicate that only 0.08 Btu/ft^2 sec can be absorbed by the water vapor. Approximately one-half of this heat would be emitted if the gas temperature is assumed to be 1560° R and uniform. Thus, it appears that the radiation effects cannot be large because the above example should give the maximum absorption rate which is consistent with the experimental equipment.

The third possibility appears to explain the observed phenomena the best. However, large variations in the composition of the gas are difficult to explain on the basis of the diffusion theory. This can be shown best by a simple example.

If it is assumed that the reaction has progressed to such an extent that all of the original reactants near the heated surface have been converted to water, it can be assumed that an imaginary plane exists in the gas near the upper plate. Above this plane there is water vapor, and below the plane the original reactants are undisturbed. The rate at which the reactants diffuse across the imaginary boundary can be computed from the one-dimensional diffusion equation. Thus,

$$\frac{\partial u}{\partial t} = D \frac{\partial^2 u}{\partial y^2}$$

where u is the concentration of one reactant (mass per unit volume), t is the time, and D is the diffusion coefficient of one reactant. The diffusion coefficient for oxygen into water (0.12 sq cm/sec at 0° C, Reference 23) is used for this example. This value of the

diffusion coefficient is used purposely so that a conservative time estimate is obtained. If it is assumed that the plate separation is one centimeter, and the imaginary plane is located at the mid-point of the plate separation, the solution to the above differential equation is

$$u = u_o \left[\frac{1}{2} + \sum_{n=1}^{n=\infty} \frac{2}{n\pi} \left(\sin \frac{3}{4}\pi n - \sin \frac{\pi}{4} n \right) e^{-D\left(\frac{n\pi}{2}\right)^2 t} \cos \frac{n\pi y}{2} \right]$$

where u is the concentration of oxygen at point y and time t, and u_o is the original concentration of oxygen below the imaginary plane. The values obtained from this equation predict that the oxygen concentration adjacent to the upper surface will be 99 percent of its equilibrium value in four seconds. The actual process should reach this value in a shorter time because the variation in the diffusion coefficient with temperature has been neglected. Therefore, the diffusion equations indicate that the reaction should approach completion in a maximum time interval of approximately six seconds. This conclusion is not consistent with the experimental results.

For all upper plate temperatures at which experiments were conducted, no systematic change in the interference pattern was observed during the nine-second time interval following the flow shutoff. The total number of fringes and the location of corresponding fringes from interferograms taken at the same temperature often differed by approximately one fringe. However, these variations appear to be random and are probably caused by opening the combustion chamber windows or by convection currents external to the

combustion chamber. Since the total fringe number does not change during the observation period, it appears that the overall rate at which the reactants combine is much lower than that predicted by the diffusion calculations. It also appears that a concentration gradient does cause the discontinuity in the experimental temperature distribution curves.

At upper plate temperatures above approximately 1540° R (Fig. 26, curve 4), the sharp break in the computed curve is not evident. The temperature distribution curves which are computed (starting from the cold plate) on the assumption that the mixture is all hydrogen and oxygen reach a value which is much too high. This is to be expected because there is little doubt that some water has formed. However, if the temperatures are calculated starting from the hot plate on the basis of the interference pattern and the assumption that the gas is only hydrogen and oxygen, and this curve is compared to a curve computed for one-dimensional heat transfer, a fair match (Fig. 27) is found for approximately two-thirds of the plate spacing. The calculated curve has a "knee" at this point and the temperature falls to a value much too low. The break in the curve indicates that a large change in concentration may occur at this point. It is possible that the break may be aggravated by the method of extrapolation. However, it is doubtful that the extrapolation error can account for the large effect, because the break occurs at a region of the interference pattern where the fringes can be measured quite accurately.

This result indicates that the index of refraction in the hot region is about the same as that of the hydrogen-oxygen mixture. However, it is not reasonable to conclude that the mixture is hydrogen and oxygen for two reasons. First, the gas adjacent to the plate would react almost instantaneously, and second, the mixture would not have a tendency to explode when disturbed. (See page 63.)

It must be concluded that at these temperatures the mixture near the upper plate is more homogeneous than at lower temperatures, and that the mixture as a whole has an index of refraction well above that of a mixture of hydrogen and oxygen.

The fact that the gas mixture near the heated plate appears to be homogeneous at the high temperatures may be influenced by the experimental method of injecting the fuel. The gas is admitted at one side of the combustion chamber and flows six inches before reaching the observation window. The flow rates are so slow that the flow must soon become laminar, but at the point of injection some turbulence must exist. Thus at the higher temperatures more of the gas may react in this region and the products be mixed by turbulence, whereas at the lower temperatures the reaction rates are so low that the amount of fuel that can react is small.

An estimate of the extent of the chemical reaction can be gained from the experimental data. For example, at an upper plate temperature of 1615° R, 60 fringes should be observed if the mixture were all hydrogen and oxygen. Eighty fringes should be observed if the gas were all water. Sixty-nine fringes were observed experimentally,

and this number did not change during nine seconds following the flow shutoff. The fact that 69 fringes were observed experimentally indicates that approximately one-half of the gas has reacted (if it is assumed that the mixture consists of only oxygen, hydrogen, and water).

The failure of the remaining part of the mixture to react might be explained in the following ways:

1. The reaction has progressed far enough that the reaction velocities are very low because the reactants have been diluted with water. (The mixture is not explosive.)
2. A layer of water vapor persists near the upper plate because of low diffusion rates and thus decreases the reaction rate.
3. Some of the intermediate particles which appear in the reaction reach a high partial pressure and thus reduce the reaction rates.

Regarding hypothesis 1, there is no doubt that the remaining mixture is explosive, as it has been observed experimentally that the mixture in the combustion chamber will explode if disturbed. For example, if the oxygen flow is started suddenly, an explosion results. This phenomenon is observed at plate temperatures above 1560° R, and it has been found to occur as late as two or three minutes after the flow was stopped.

It is doubtful that the admitted oxygen initiates the reaction chemically as there is no surplus of hydrogen in the combustion

chamber (if it is assumed that only hydrogen, oxygen, and water are present) and the explosion and the pulse appear to be simultaneous. The reaction is probably initiated by turbulence caused by the quick pulse of oxygen. In any case, it is obvious that the mixture has not reacted to such an extent that it is not explosive.

Hypothesis 2 can be excluded from consideration of the following observations. It is quite conclusive that water is formed near the upper plate if the temperature is above the explosion limit. Thus, it would appear reasonable to assume that nothing but water is present in the portion of the gas which is at a temperature considerably in excess of the explosion limit. However, if the temperature of the gas is computed from the hot plate on the assumption that the gas in this region is water, a temperature curve is obtained (Fig. 27) which is much too flat when compared with a curve computed from the one-dimensional heat transfer equations for a stoichiometric mixture ratio of hydrogen and oxygen. If the gas in the vicinity of the heated surface is water, the temperature should fall more rapidly than predicted from the previous computation because the thermal conductivity of water vapor is approximately one-half that of the mixture. Therefore, the gas near the upper surface cannot be all water, but must be a mixture whose composite index of refraction is considerably lower than that of water vapor alone. These conclusions appear reasonable because the interference pattern is quite accurate in this region. The extrapolation error is eliminated when the temperature is computed from the upper plate,

and the refraction effects are the smallest in the hot region.

The low index of refraction could be accounted for by assuming that approximately sixty percent of the gas in the hot region is hydrogen. The fact that hydrogen has such a high diffusion coefficient may allow the partial pressure of the hydrogen to be essentially constant in the entire space. It should be noted that a variation in relative concentrations of oxygen and hydrogen is predicted by the Chapman effect (24). This theory predicts the partial separation of a bimolecular mixture which is placed in a temperature gradient. The heavy molecules migrate toward the cooler portion of the vessel and the lighter molecules toward the hotter portion of the vessel. Applying this theory to these experimental data, a relative difference in concentration of approximately ten percent is predicted for a hot plate temperature of 1615° R. This variation in concentration is probably large enough to affect the reaction rate but does not appear to be large enough to explain the observed phenomena. However, the above example is computed for equilibrium conditions. Thus, if the oxygen is continually removed in the reaction zone so that the concentration in the hot region is virtually zero, it is possible that the Chapman effect might decrease the diffusion velocity of the oxygen and thus decrease the reaction rates.

Thus, it can be concluded that the gas near the heated surface is not all water, but it is doubtful that enough hydrogen is available to account for the low index of refraction.

Considering the third hypothesis, there is specific evidence (25) that the hydrogen atom is destroyed in the reaction $H + O_2 + M = HO_2 + M$ (where M is a third body), if there is an excess of hydrogen atoms, and if the reaction temperature is not too high. The HO_2 particle is immediately reduced to H_2O_2 by the reaction $HO_2 + H_2 = H_2O_2 + H$. The number of H_2O_2 particles found in a given experiment has been observed in special cases to amount to about three times that of the water formed.

All the conditions for this reaction are present in the given experimental equipment. The higher diffusivity of hydrogen combined with the Chapman effect would tend to cause a surplus of the hydrogen molecules in the hot region where a high concentration of hydrogen atoms would be favored by the higher temperature. These hydrogen atoms would tend to diffuse toward the cold plate very rapidly because of their high diffusion coefficient. The hydrogen atoms could then react with the oxygen molecules near the interface between the water and the mixture. This reaction may be very important because the oxygen diffuses slowly into this region and three-body collisions are important.

It should also be noted that the yield of this reaction depends upon the third body. Von Elbe and Lewis have found that the water molecule is about fifteen times as efficient as the other molecules in initiating the combination. This reaction may also take place to a large extent in the portion of the chamber where the gas is admitted. Approximately one-half of the gas flows toward

the hot plate as it is injected. This gas will pass near the hot surface where the high temperature and turbulence would favor the reaction. A large portion of this gas must then flow down toward the cool surface where the intermediate component H_2O_2 can be "frozen".

It has been suggested that some of the intermediate particles might also be formed in a region of the combustion chamber where the temperature is quite low. This process is similar to that which occurs in the "hot-cold" tube experiments (27). The "freezing" of the intermediate particles apparently results from the selective diffusion of the very high velocity particles. These particles originate near the heated surface and diffuse into a region where the temperature is low enough that the particle resulting from the reaction is stable. Thus it is possible that some of the intermediate particles will be "frozen" near the lower plate. The concentration of these particles would be governed by the difference between the rate at which they are formed and the rate at which they diffuse toward the upper surface. The influence of the Chapman effect on the concentration distribution of the H_2O_2 particles is probably greater than its influence on the distribution of the oxygen. Thus, it may be possible to have a large concentration of H_2O_2 near the lower surface. This effect may explain the apparent change in concentration near the cool surface.

Thus it appears that the mechanism for forming H_2O_2 molecules is present. It also appears that the hydrogen peroxide can exist

without excessive thermal dissociation at all temperatures present in the experimental apparatus. This is concluded from a calculation of the equilibrium constant K_p for the following dissociation reaction.

$$H_2 + O_2 \rightleftharpoons H_2O_2$$

The equilibrium constants at 1530° R and 720° R are 1.446×10^2 and 7.43×10^{12} respectively. Thus, approximately twenty-five percent of the H_2O_2 would be dissociated in the hottest region of the combustion chamber. Thus, it is possible for the H_2O_2 molecules to reach a large concentration in the combustion chamber if the reaction $H_2 + H_2O_2 = 2H_2O$ is neglected. A computation of the equilibrium coefficients for this reaction indicates that there is a very strong tendency for the reaction to go toward water. However, the equilibrium constants for the hydrogen-hydrogen peroxide reaction do not indicate the rate at which the reaction will proceed. Therefore, it may be possible for the hydrogen-peroxide to reach a concentration which is large enough (thereby decreasing the O_2 concentration) to slow the reaction considerably. This explanation cannot be picked with certainty, as the composition of the gas in the combustion chamber cannot be determined with the present equipment.

It appears from the preceding discussions that the following idealized mechanism may explain the suppression of the explosion. Assume that it is possible to heat the mixture in a very short time so that the upper plate temperature is actually above the explosion limit of the gas, and the temperature gradient in the gas is

established before the reaction has progressed an appreciable amount. Then the layer of the mixture near the hot surface will react very quickly. The product of this reaction will probably be water. However, the temperature gradient is so steep that the heat liberated during the reaction is small compared to the heat which is passing through the mixture due to thermal conduction. Thus the heat of reaction cannot raise the temperature of the cooler layer below the reacting layer enough to make it react rapidly. The thickness of the reacting layer probably will be such that its lower surface is at a temperature slightly below the explosion limit of the mixture. At this time, there is nothing but water in the hottest region of the combustion chamber and the reaction can continue by diffusion only. Since the hydrogen can diffuse into the water vapor approximately seven times faster than the oxygen, the hydrogen will have reached a high concentration before a great deal of oxygen has diffused into the water layer. It appears that the reaction should proceed at a rate governed by the diffusion of oxygen into the hot region of the chamber. Theoretically, this process should approach completion in approximately six seconds. Experimentally it has not approached completion in two minutes. Thus it is evident that either the oxygen and hydrogen are not diffusing at the expected rate, or that the hydrogen-peroxide reaction is predominating.

In summarizing the discussion of this investigation, the following statements can be made.

The method used to gain information regarding the reaction

mechanism appears on the whole to be satisfactory. The interferometer gives results which are reproducible within approximately five percent. The accuracy can probably be improved by replacing the combustion chamber shutters with quartz windows. The response of the interferometer was not utilized in this investigation because the reaction rates are much slower than those expected. The utility of the interferometer is also limited in this case because of the inability to obtain the composition of the gas mixture. It was very valuable, however, for detecting the temperature at which a reaction appears. It was also very useful in estimating the composition of the mixture near the upper surface.

The results of this investigation indicate that either of two phenomena may suppress the ignition of the combustible mixture. First, the gases may be stratified within the combustion chamber, the slow reaction being attributed to very slow diffusion rates which may be caused by the Chapman effect. Second, the concentration of some of the more stable intermediate particles, especially the H_2O_2 molecule, may be quite large. This effect would rapidly decrease the concentration of oxygen.

Neither of these processes can be picked with certainty because of limitations of the present test equipment.

VIII. CONCLUSIONS

It is possible (within the temperature range covered by this investigation) to suppress the explosion of a stoichiometric mixture of hydrogen and oxygen. This is accomplished by placing the mixture in a shallow rectangular combustion chamber, the upper surface of which is heated. The lower surface is maintained at a temperature of 550° R.

No chemical reaction is observed at a plate temperature below $1500^{\circ} \pm 10^{\circ}$ R. This temperature is the temperature of the explosion limit at atmospheric pressure.

Theoretical reaction rates computed from the thermal equilibrium concentration of the hydrogen atom agree favorably with the experimental values which were obtained from Von Elbe and Lewis' data. It is evident from the results of this calculation that the hydrogen atom is the primary chain carrier.

When the upper plate temperature is higher than the explosion limit temperature, the overall rate at which chemical combination takes place should depend directly upon the rate at which fresh reactants are diffusing into the region near the heated surface.

The observed rate of chemical combination is much lower than that predicted from the one-dimensional diffusion equations. The composition of the mixture was found to be constant during the nine-second time interval following the cessation of flow. This condition was observed for all upper plate temperatures at which experiments were conducted.

The suppression of the reaction may be attributed to either of

two causes:

1. The reactants do not diffuse into the water layer at a rate consistent with the diffusion theory. This may be caused by the Chapman effect.
2. A high concentration of the intermediate component H_2O_2 is present which decreases the partial pressure of the oxygen and thus reduces the reaction rate.

The exact mechanism which causes the suppression of the explosion cannot be ascertained because of limitations of the equipment available.

IX. PROPOSAL FOR FURTHER RESEARCH

The most interesting course for further research falls along two lines. First, the composition of the mixture which exists in the combustion chamber and the concentration of these components as a function of the distance between the plates should be determined. Second, after the components are identified, the manner in which they are formed should be investigated.

The actual composition and the composition gradient might be determined by an absorption technique. This is done by passing separate light beams through the mixture having frequencies which match the absorption spectrum of one or more of the components which are present. The concentration gradient is determined by measuring the intensity of the transmitted beam as a function of the location between the plates. The possibility that a photochemical reaction will also accompany the absorption of the radiation must also be considered.

Another possible method of determining the composition of the mixture is that of gas sampling. This is done by allowing the sample to flow into an evacuated vessel. The assumption is that the actual components present are "frozen". The composition is then determined by mass spectroscopy or one of the conventional gas absorption techniques.

If it is assumed that the composition can be continuously observed, the mechanism by which the intermediate particles are formed could be observed experimentally in two ways. First, the explosive mixture would be passed through the combustion chamber steadily, and the location at which the composition change occurs is observed as

the upper surface of the chamber is heated. In this way, it could be determined if the intermediate particles are formed near the heated surface and diffuse downward, or if they are formed in the cool mixture by the very high velocity particles which diffuse from the upper surface. This technique has the advantage of being a steady flow process so that an equilibrium condition can be observed at any temperature. The disadvantage of the method results from the fact that the formation mechanism would be confused by flow effects.

The second possible method would be to place a homogeneous mixture in the combustion chamber and then heat one surface very rapidly. In this manner, the flow effects would be eliminated. The rapid temperature change might be accomplished by depositing a very thin layer of metal on the surface of a good insulator such as quartz. This surface would then be heated by passing an electric current through the metal film.

The effect of the temperature gradient upon the overall rate at which the reactants are consumed, and the effect of the temperature gradient upon the position between the two plates where the intermediate particles appear should also be investigated.

It should also be noted that the experimental equipment could be used for investigations of the following type with very few modifications.

1. Two-dimensional convective heat transfer.
2. Boundary layer studies.
3. Studies of the effect of heat transfer upon the boundary layer.

X. APPENDIX I

DERIVATION OF FRINGE CONSTANTS

The relation between the interference pattern and temperature distribution within the combustion chamber can be easily deduced with the aid of a simple diagram (Fig. 29).

It is assumed that the temperature along the length of each light path is uniform and that the light travels in straight lines. (Refraction effects are neglected.)

The line labeled T_1C_1 refers to the undisturbed ray of light passing through air at room temperature T_1 and composition C_1. The lines labeled T_2C_2 and T_3C_2 are rays passing through the gas of composition C_2 in the combustion chamber.

The number of wave lengths of light in path 1 is

$$N_1 = \frac{L}{\lambda_1} = \frac{L}{\lambda_o} n_1 \qquad (1)$$

where n_1 is the index of refraction of the gas along path 1, λ_o is the wave length of the light in a vacuum, and L is the length of the combustion chamber.

Similarly,

$$N_2 = \frac{L\ n_2}{\lambda_o}\ ;\quad N_3 = \frac{L\ n_3}{\lambda_o}\ . \qquad (2)\ (2a)$$

If the substance in the combustion chamber is different than 1, N_2 will be different from N_1, even if $T_1 = T_2$. This difference is not observed on the interferogram because the difference merely corresponds to a difference in effective path length and has no relation to the temperature distribution within the chamber. Thus,

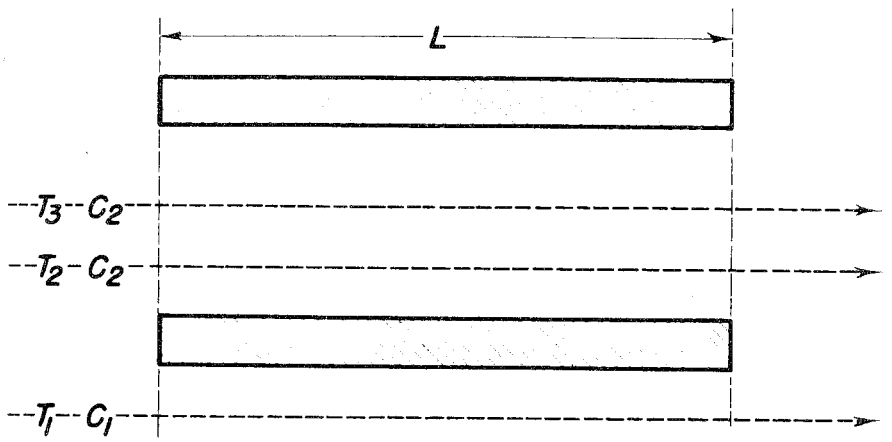

FIGURE 29

Schematic diagram of light paths

the number of fringes actually observed is

$$N = (N_1 - N_3) - (N_1 - N_2) = N_2 - N_3 \ , \tag{3}$$

and is independent of the conditions exterior to the combustion chamber.

Substituting (2) and (2a) into equation (3), the following relation is obtained:

$$N = \frac{L}{\lambda_o} (n_2 - n_3). \tag{4}$$

The index of refraction for gases can be approximated accurately by the expression

$$n = 1 + k\rho \ , \tag{5}$$

where k is a constant of the gas and ρ is the density of the gas.

Substituting (5) into (4) and remembering that $k_1 = k_2$, the relation

$$N = \frac{Lk}{\lambda_o} (\rho_2 - \rho_3) = \frac{Lk\,\rho_2}{\lambda_o} \left(1 - \frac{\rho_3}{\rho_2} \right) \tag{6}$$

is obtained. The relation $\rho_3/\rho_2 = T_2/T_3$ is valid if the perfect gas relation holds and the pressure is constant within the apparatus.

Thus the desired relation between T and N is obtained.

$$N = \frac{Lk\,\rho_2}{\lambda_o} \left[1 - \frac{T_2}{T_3} \right] . \tag{7}$$

In this particular application it is more desirable to have T_3 as a function of N since the data are more easily evaluated in this way.

Solving (7) for T_3, the final relation is found.

$$T_3 = \frac{T_2}{1-N/\beta} \tag{8}$$

where T_3 = temperature at the Nth fringe, T_2 = temperature of the cold plate, and $\beta = \frac{Lk\,\rho_2}{\lambda_o} = \frac{Lk}{\lambda_o}\,\frac{P_o}{RT_2}$, where P_o is standard atmospheric pressure and R is the gas constant.

The equation was evaluated by plotting curves of T_3 as a function of N with T_2 as a parameter. This is necessary since β is a function of T_2.

The constant β was evaluated at various values of T_2. The values of k were obtained from the International Critical Tables (26). The values which were used are tabulated below.

Air - $(n-1) = 270.6 \times 10^{-6}$ @ 0° C.

H_2 - $(n-1) = 139.66 \times 10^{-6}$ @ 0° C.

O_2 - $(n-1) = 271.70 \times 10^{-6}$ @ 0° C.

H_2O vapor - $(n-1) = 252.7 \times 10^{-6}$ @ 0° C.

The value of (n-1) for the mixture of H_2 and O_2 is obtained by adding the value of (n-1) of each gas after it has been weighted in direct proportion to its partial pressure. The calculated curves of T as a function of N are shown in Fig. 30.

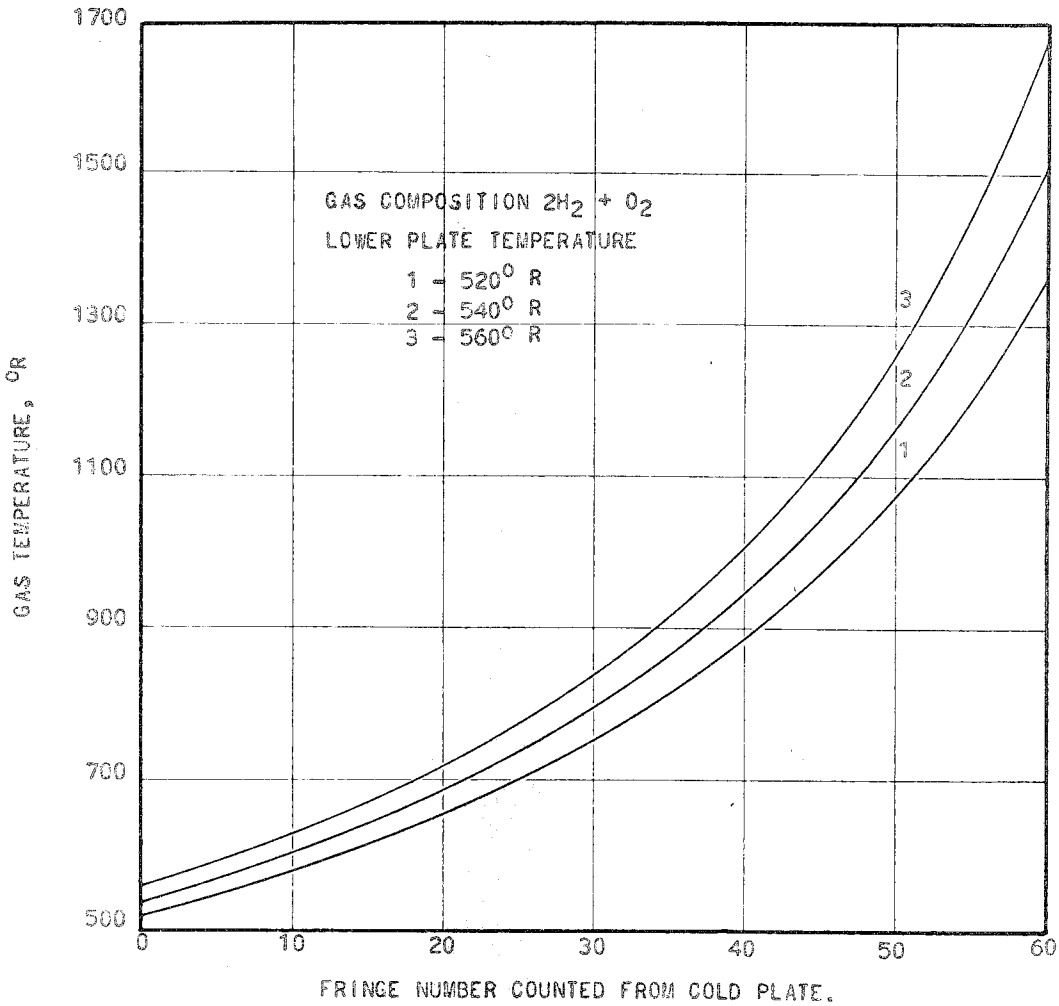

FIG. 30 THEORETICAL GAS TEMPERATURE AS A FUNCTION OF THE NUMBER OF FRINGES.

XI. APPENDIX II

CORRECTIONS FOR REFRACTION

It has been stated that an image of the cold plate can never be obtained because of the refraction of the light beam passing through the combustion chamber. The reasons for this can be seen by referring to Fig. 31. The light entering the combustion chamber is given a small positive slope to minimize the distortion of the image. The light passes through the combustion chamber on a curved path and leaves with a negative slope. After leaving the combustion chamber, the light travels in a straight line. Because the camera lens does not allow for the past history of the light, the bottom ray appears to originate at point 3 in the focal plane and is focused at 3' on the image. If the slope of each ray leaving the combustion chamber is exactly the same, the refraction simply causes a shift of the image. This is not the case because the density of the gas and hence the index of refraction is inversely proportional to the absolute temperature of the gas. Therefore, the gradient of the index of refraction (dn/dy) is greatly reduced near the upper plate and the exit slope of a ray passing near the upper plate is not as great as a ray near the lower plate. This can be seen graphically in Fig. 31. Points 2' and 4' indicate the image positions of two imaginary rays passing through the apparatus, and 3' and 1' give the location of the actual light rays. The image is compressed on the cold plate side and the resulting interferogram must be corrected before an accurate temperature distribution can be obtained.

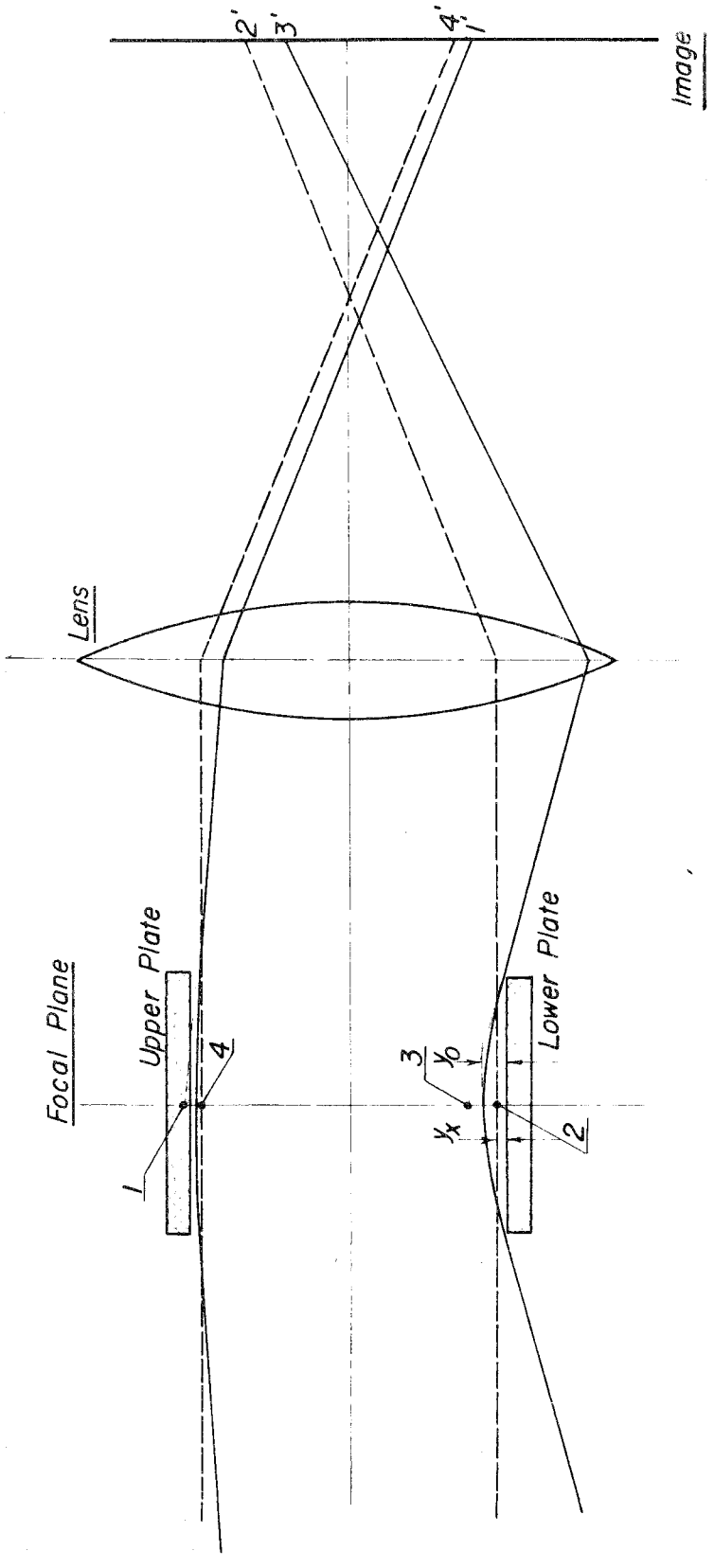

FIGURE 31

Refraction error

Each fringe location must be further corrected to compensate for the temperature variation along the light path. As seen from Fig. 32, the bottom ray travels on a symmetrical curved path (the initial slope being correct) and thus travels through continuously varying densities. The number of wave lengths in this path is an integral over all increments of length along the path and thus has the same number of wave lengths as an imaginary horizontal path at a height (y*) above the cold plate.

These corrections are deduced by finding the value of y* for each ray, and the slope of the light rays emerging from the combustion chamber (Fig. 32). This is done in the following manner: it is assumed that the angle of the light at the entrance can be adjusted so the paths of the two extreme rays are symmetrical within the combustion chamber. It is not possible to satisfy the conditions on the entering light which make each light path within the combustion chamber symmetrical. This is true since the required slope for a symmetrical path is a nonlinear function of y, whereas a simple lens gives a linear variation of slope. The equation of the path is derived and the values of y at the exit (y_{ex}) and the exit slope $(dy/dx)_{ex}$ for several y_o's is computed, where y_o is the height above the lower plate at which the slope of a given ray is zero. The apparent necessary correction is then $\Delta' = \left[\mathcal{E} + (y_{ex} - y^*)\right]$ (Fig. 32). The true value of the displacement on the image is the apparent shift (Δ') minus the displacement of the image of the upper plate (Fig. 33). Hence, the true correction is then given

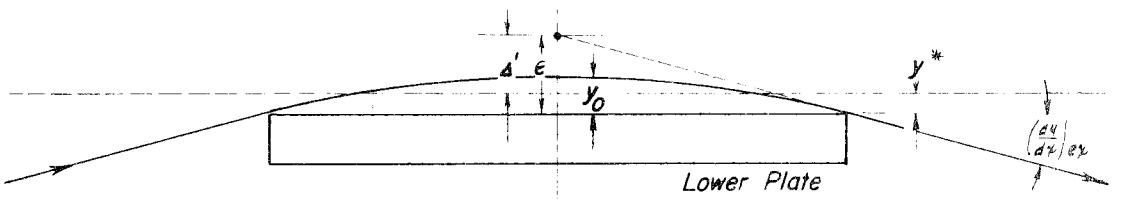

FIGURE 32

Path of ray at lower plate

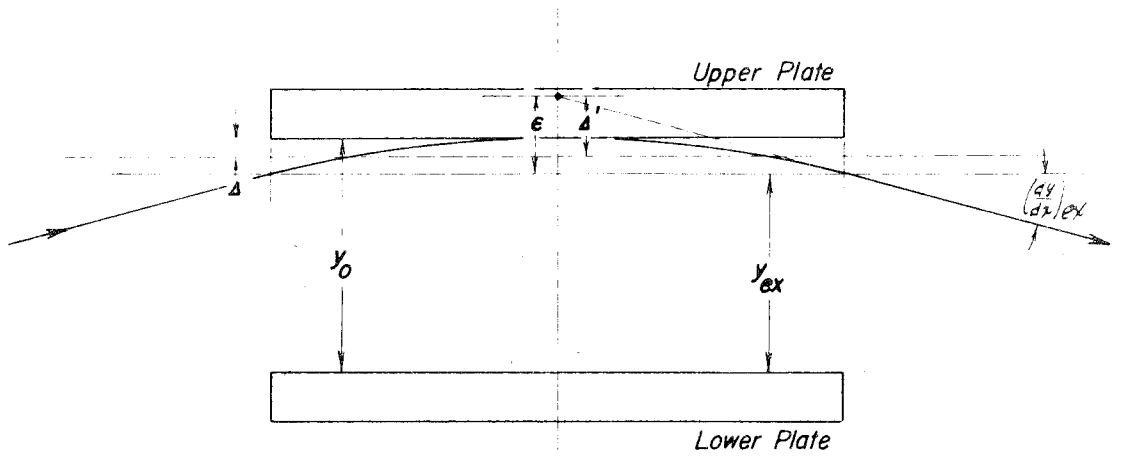

FIGURE 33

Path of ray at upper plate

by the following relation:

$$\Delta_y = \Delta' - \xi$$

$$\Delta_y = (\mathcal{E} + y_{ex} - y^*)_y - (\mathcal{E} + y_{ex} - y_o)_{y_o} = 1$$

where ξ is the displacement of the image of the upper plate and Δ_y is the correction which must be made at a distance y above the lower plate. The values of y are dimensionless numbers such that the plate separation is assigned a value of y = 1. The corrections for the intermediate rays are done in a similar manner, the asymmetry of the path being taken into consideration.

Derivation of the Refraction Equations.

The equation of the curve along which a light ray travels as it passes through the combustion chamber is found by considering a curve in space relative to an arbitrary coordinate system (Fig. 34). Consider a segment ds of the light path a-a, and investigate the dependence of the radius of curvature R upon the gradient of the index of refraction normal to this segment.

The time dt required for the light to travel the distances ds and ds' is the same because the elements of length dR lie in the wave front. Thus,

$$ds = v\,dt; \quad ds' = v'\,dt \qquad (1)$$

The velocities v and v' are related to the indices at these points by the relations $v = c/n$, and $v' = c/n'$ respectively. The index of refraction along the segment ds is n and the index of refraction along the segment ds' is n'. The relation between n and n'

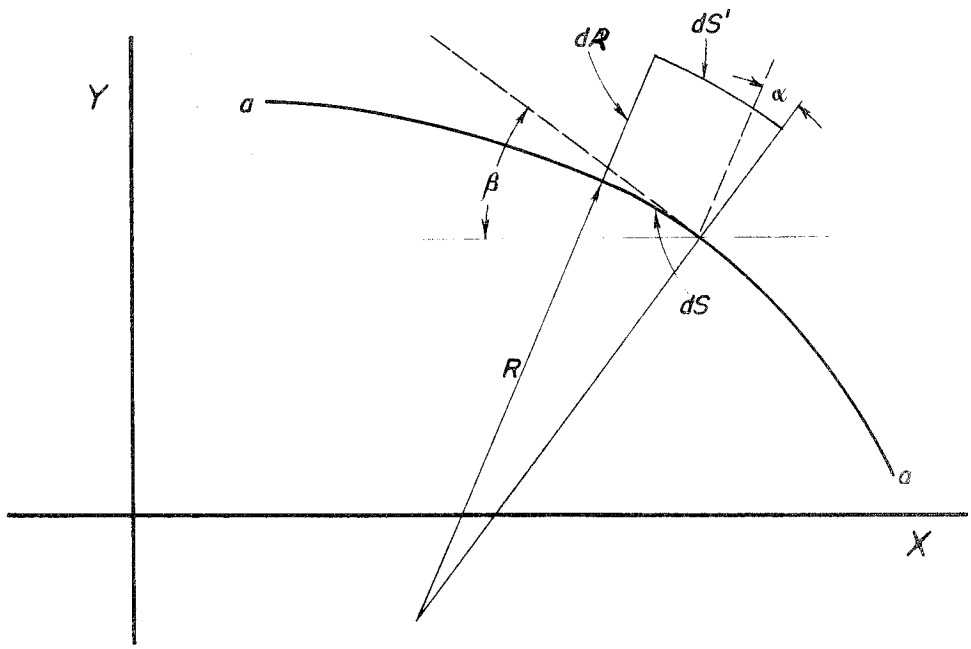

FIGURE 34

Derivation of light path

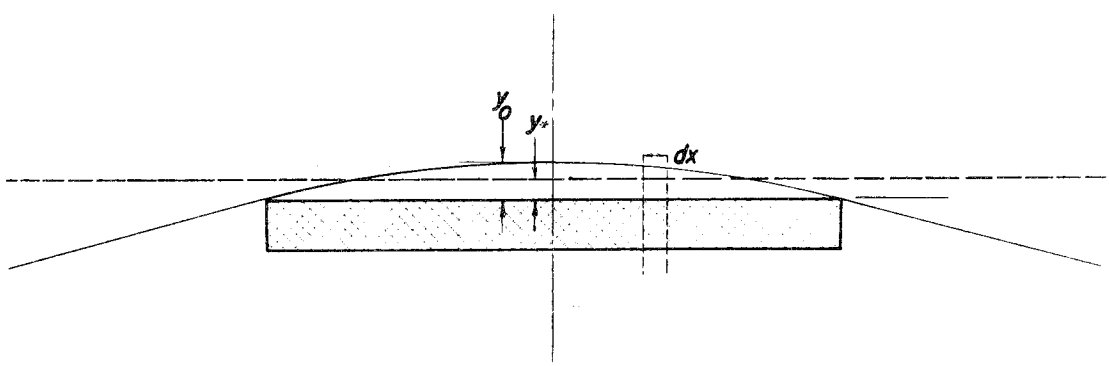

FIGURE 35

Correction for nonuniform temperature

is obtained from the partial derivative of n with respect to R. Thus,

$$n' = n + \frac{\partial n}{\partial R}\, dR \tag{2}$$

The angle α is given by the relation

$$\alpha = \frac{ds' - ds}{dR} = \frac{c\, dt}{dR}\left(\frac{1}{n'} - \frac{1}{n}\right). \tag{3}$$

Substituting equation (2) into equation (3), it is found that

$$\alpha = \frac{c\, dt}{dR\, n}\left(\frac{1}{1 + \frac{\partial n}{\partial R}\,\frac{dR}{n}} - 1\right) = \frac{c\, dt}{n\, dR}\left[\frac{-\frac{\partial n}{\partial R}\,\frac{dR}{n}}{1 + \frac{\partial n}{\partial R}\,\frac{dR}{n}}\right]. \tag{4}$$

Expanding the denominator of equation (4) in a series,

$$\alpha = \frac{c\, dt}{n^2\, dR}\left[-\frac{\partial n}{\partial R}\, dR\right]\left[1 - \frac{\partial n}{\partial R}\,\frac{dR}{n} + \left(\frac{\partial n}{\partial R}\,\frac{dR}{n}\right)^2 + \cdots\right]. \tag{5}$$

Since n is of the order of one, and experimentally $\partial n/\partial R$ is small compared to one, terms in equation (5) involving $(\partial n/\partial R)^2$ can be neglected. Now

$$\alpha = \frac{c\, dt}{n^2\, dR}\left(-\frac{\partial n}{\partial R}\, dR\right). \tag{6}$$

This equation can be transformed to the variables x and y by substituting the relation between α and (d^2y/dx^2).

Since $R\alpha = ds$ (Fig. 34) and $d^2y/dx^2 = -1/R$, equation (6) reduces to

$$-\frac{d^2y}{dx^2}\, ds = \frac{1}{n}\left(\frac{c\, dt}{n}\right)\left(-\frac{\partial n}{\partial R} \cdot dR\right)\frac{1}{dR}. \tag{7}$$

Equation (7) can be reduced further by using the relation $ds = c\, dt/n$. Thus,

$$\frac{d^2y}{dx^2} = \frac{1}{n}\,\frac{\partial n}{\partial R} \tag{8}$$

The term $\partial n / \partial R$ in equation (8) is evaluated by assuming that n if a function of y only. Therefore,

$$\frac{dn}{dR} = \frac{dn}{dy} \cos \beta = \frac{dn}{dy} \sqrt{\frac{1}{1 + \left(\frac{dy}{dx}\right)^2}} \tag{9}$$

Substituting equation (9) into equation (8), the differential equation of the light path is obtained.

$$\frac{d^2y}{dx^2} \sqrt{1 + \left(\frac{dy}{dx}\right)^2} = \frac{1}{n} \frac{dn}{dy} \tag{10}$$

For this application, the differential equation can be simplified by neglecting $(dy/dx)^2$ compared to one. This assumption is justified by the final solution, as (dy/dx) for the values of x bounded by the combustion chamber is never larger than 0.04 radians.

The equation of the path is then

$$\frac{d^2y}{dx^2} = \frac{1}{n} \frac{dn}{dy} . \tag{11}$$

The term dn/dy is replaced with a function of y by assuming that the temperature distribution between the plates is linear. This assumption is justified on the basis of the experimental data (Fig. 25). The temperature distribution differs from a linear relation because of three effects: First, the thermal conductivity varies with temperature, second, heat is added to the gas in the reaction zone, and third, there is a difference in the composition of the gas near the hot plate after the reaction has started. However, these effects do not cause the actual temperature curve to deviate more than 15 percent from a straight line.

The functional relation between n and y is

$$n = 1 + \frac{k'}{T} = 1 + \frac{k'}{T_o + Dy} \quad . \tag{12}$$

where $k' = k\ P_o/R$ (Appendix I), T_o is the temperature of the cold plate, and D is a constant whose value depends upon the hot plate temperature.

Substituting the value of dn/dy into equation (11), the following relation is obtained.

$$\frac{d^2y}{dx^2} = - \frac{k'D}{(T_o + Dy)^2 + k' (T_o + Dy)} \quad . \tag{13}$$

This equation can be reduced to a differential equation of the first order by the substitution

$$A = dy/dx;\ dA/dy = 1/A\ d^2y/dx^2 \quad . \tag{14}$$

Equation (13) now becomes

$$AdA = - \frac{k'D\ \ dy}{(T_o + Dy)^2 + k' (T_o + Dy)} \quad , \tag{15}$$

and the first integration gives the solution

$$- \frac{A^2}{2} = \log \left[\frac{2\ Dy + 2\ T_o}{2\ Dy + 2\ T_o + k' + k'} \right] + F$$

$$= \log \left[\frac{y + T_o/D}{y + \frac{T_o + k'}{D}} \right] + F \tag{16}$$

where F is a constant which is determined by the boundary conditions.

Equation (16) cannot be solved in closed form, but can be simplified by another approximation. Rearranging equation (16),

$$-\frac{A^2}{2} = \log\left[\frac{1}{1 + \frac{k'}{aD}}\right] + F \tag{17}$$

where $a = (y + T_o/D)$ and has a minimum value of 0.50. The maximum value of k'/D is approximately 10^{-4}. Thus, the second term in the denominator has a maximum value of approximately 2×10^{-4}, and a reasonable approximation can be obtained by expanding equation (17) in a power series. Neglecting second order terms, equation (17) becomes

$$-\frac{A^2}{2} = -\frac{k'}{aD} + F \tag{18a}$$

or

$$A = \pm \sqrt{2}\ \sqrt{-F + \frac{k'}{yD + T_o}}\ . \tag{18b}$$

Separating the variables and rearranging, equation (18) can be written as

$$-\sqrt{2}\ dx = \frac{\sqrt{yD + T_o}\ \ dy}{\sqrt{F(yD + T_o) + k'}} \tag{19}$$

the solution of which is

$$\sqrt{2}\ x\ (DF) = \sqrt{(yD + T_o)\left[k' - F(yD + T_o)\right]}$$

$$-\frac{k'}{2\sqrt{F}} \sin^{-1}\left[1 - \frac{2F(yD + T_o)}{k'}\right] + G \tag{20}$$

where G is the second constant of integration.

This equation was evaluated using the following boundary conditions:

$$x = 0,\ (dy/dx) = 0$$

$$x = 0,\ y = y_o \tag{21}$$

Thus, the integration constants are

$$F = \frac{k'}{y_o D + T_o}$$

$$G = \frac{k'}{2\sqrt{F'}} \sin^{-1}(\quad -1) \tag{22}$$

The constant G has an infinite number of values depending upon which value of the arc sine is chosen. Mathematically, these values of G correspond to the various loops of the repeating solution. The desired value of G is that value which will give the minimum positive value of x for a given value of y. This value of G is

$$G = \frac{k'}{2\sqrt{F'}}\left(\frac{3}{2}\pi\right). \tag{23}$$

Substituting the values of the integration constants into equation (20), the final relation is obtained.

$$\sqrt{2'} \times (DF) = \sqrt{k' (yd + T_o)\left[1 - \frac{yD + T_o}{y_o D + T_o}\right]} - \frac{k'}{2\sqrt{F'}}\left[\frac{3}{2}\pi - \sin^{-1}\left(1 - \frac{2(yd + T_o)}{y_o D + T_o}\right)\right] \tag{24}$$

The values of y_{ex} and $(dy/dx)_{ex}$ were obtained from equation (24) by calculating x as a function of y for ten dimensionless values of y_o varying from 0.02 to 1.00. This solution was carried out for four temperatures of the upper plate. The temperature of the lower plate was taken to be constant and a value of 550° R was used. These curves were plotted and the value of y_{ex} for each value of y_o was taken from the graph. The paths of the intermediate rays were found by computing the value of x for a given y_o, at which the slope of the ray was the

same as that from the light source. The coordinates were then shifted so this value of x corresponded to the entrance of the combustion chamber. The values of $(dy/dx)_{ex}$ corresponding to the values of y_{ex} and y_o were obtained from equation (18b). The value of $\mathcal{E}$ (Fig. 32) for this particular ray is $(L/2)\left[(dy/dx)_{ex}\right]$.

It has been assumed in this discussion that the origin of the coordinate system for the extreme rays is at the center of the lower plate. This location gives the minimum value of $\mathcal{E}$, and thus the least distortion of the image. This is demonstrated as follows: each ray entering the combustion chamber is refracted downward, the slope of the ray continuing to decrease more rapidly as it progresses. Thus, under normal operating conditions, it was found that if the slope of the ray was taken to be zero at the entrance of the combustion chamber, the first ray which could pass through the chamber without striking the lower plate entered at approximately one-tenth of the plate separation. This arrangement is very undesirable, as the slope of the ray at the exit is large, giving a value of $\mathcal{E}$ nearly twice the value obtained when the coordinate system is located at the center of the plate. Furthermore, this ray travels through gas having very different temperatures and it is therefore difficult to deduce the actual temperature distribution from these measurements.

The value of y* for a given y_o is the height above the lower plate of the path of a hypothetical ray passing straight through the combustion chamber. The imaginary path contains the same

number of wave lengths as the corresponding actual path passing through y_o. Thus, this value of y* gives the location relative to the lower plate of the plane which is at the temperature which the ray passing through y_o indicates.

This correction is obtained as follows: Consider the elements of length dx of the actual path and the equivalent path (Fig. 35). It is assumed that these distances are of the same length. This is an approximation, but is quite accurate because of the small angles involved. The number of wave lengths in the actual path element is

$$dN_a = \frac{dx}{\lambda_a} = \frac{dx}{\lambda_o} \cdot n_a \tag{25}$$

and the number of wave lengths in the element of the equivalent path is

$$dN^* = \frac{dx}{\lambda^*} = \frac{dx}{\lambda_o} \; n^* \tag{26}$$

where λ_a and λ^* are the wave lengths of the light along the actual path, and the equivalent paths respectively. Similarly, n_a and n* are the indices of refraction along these paths.

To avoid taking differences of very large numbers, it is desirable to take the difference of the quantities given in equations (25) and (26) before integrating over the path length.

Combining equations (25) and (26), the relation for the symmetrical paths is

$$N = 2\int_o^{L/2} (dN^* - dN_a) = \frac{2}{\lambda_o}\int_o^{L/2} (n^* - n_a)\, dx \tag{27}$$

where N is the difference in the number of wave lengths in the two

paths. Since this number is zero for the correct equivalent path, equation (27) is integrated, the left-hand side equated to zero, and the value of n*, and therefore y* which satisfies the condition is determined. The integration can be performed after substituting the functional relation of the indices, and changing the variable from x to y. Equation (27) becomes

$$N = \frac{1}{\lambda_o \sqrt{2}} \int_{y = y_o}^{y = y_{ex}} \left(\alpha - \frac{k'}{yD + T_o} \right) \frac{\sqrt{yD + T_o}}{\sqrt{k' - F(yD + T_o)}} \, dy \qquad (28)$$

where $\alpha = (n^* - 1) = k'/y^*D + T_o$ and $k'/(yD + T_o) = (n_a - 1)$. The integration of equation (28) can be simplified by changing the variable to $\Gamma = yD + T_o$. Substituting and changing the limits, equation (28) becomes

$$N = \frac{1}{\lambda_o \sqrt{2}\, D} \int_{\Gamma = y_o D + T_o}^{\Gamma = y_{ex} D + T_o} \frac{(\alpha\Gamma - k')}{k'\Gamma - F\Gamma^2} \, d\Gamma \qquad (29)$$

the solution of which is

$$N = \frac{1}{\lambda_o \sqrt{2}\, D} \left[- \frac{\sqrt{\alpha k' - F\Gamma^2}}{F} - \frac{k(\alpha - 2F)}{-2F} \left\{ - \frac{1}{\sqrt{F}} \sin^{-1} \left(\frac{k' - 2F}{k'} \right) \right\} \right]_{\Gamma = y_o D + T_o}^{\Gamma = y_{ex} D + T_o} \qquad (30)$$

Equating the left-hand side of equation (30) to zero, substituting the limits and simplifying, the final relation is

$$y^*D + T_o = \frac{\frac{1}{2\sqrt{F}} \left[3/2\,\pi - \sin^{-1} \left(1 - \frac{2(y_{ex}D + T_o)}{y_o D + T_o} \right) - \sqrt{k'T_o - FT_o^2} \right]}{\sqrt{F} \left[3/2\,\pi - \sin^{-1} \left(1 - \frac{2(y_{ex}D + T_o)}{y_o D + T_o} \right) \right]} \qquad (31)$$

The value of the arc sine must again be picked to give an answer having a physical meaning. Only one of the different values of y* obtained from these values of the arc sine has any meaning in this case. This is true because the original assumption that the slope of the actual path is small is not justified if the integration is carried to the second loop of the mathematical curve. The values of y* for the nonsymmetrical paths are found from the same equations by using the proper limits in the integration.

The final correction is then obtained in the manner previously outlined. The graph of the complete correction as a function of y for several upper plate temperatures is shown in Fig. 36.

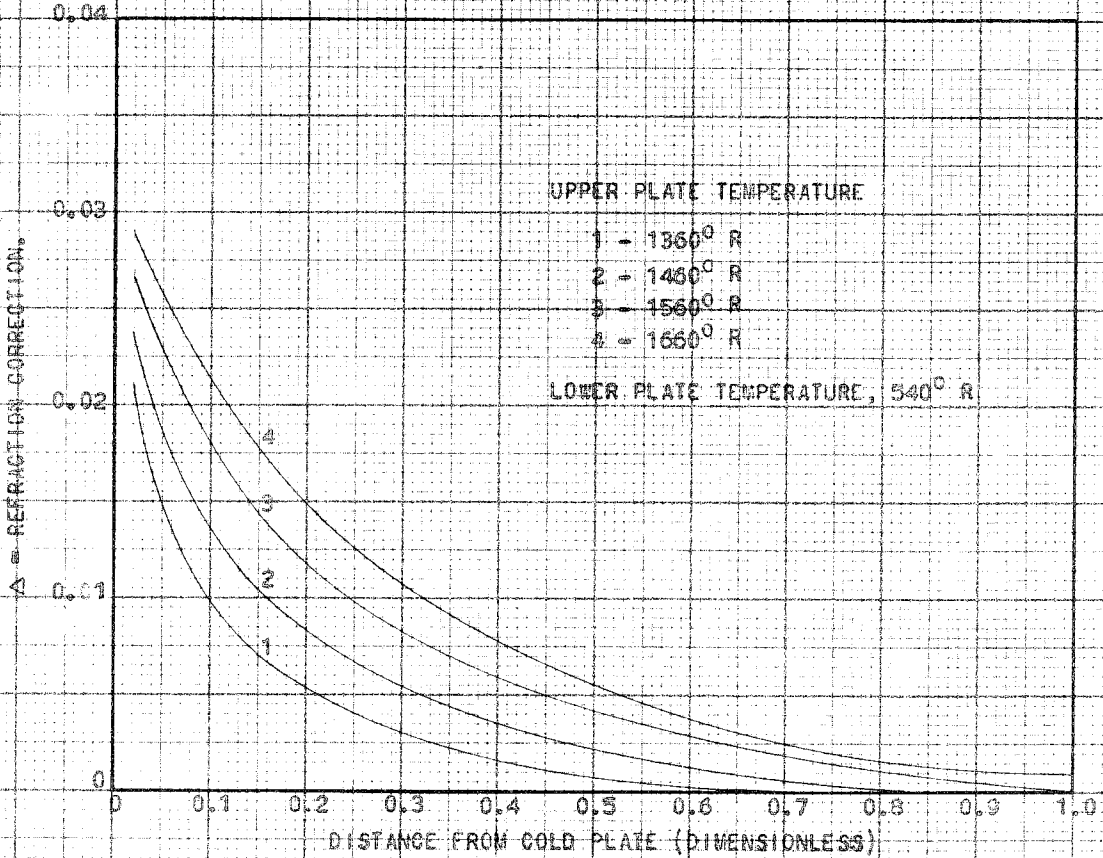

FIG. 36 CALCULATED REFRACTION CORRECTION.

XII. APPENDIX III

METHOD OF INITIAL ADJUSTMENT OF THE INTERFEROMETER MIRRORS

A method for making the initial adjustments to the interferometer mirrors is outlined in references 16 and 17. Since these papers are not readily available and in some cases the technique is vague, the method will be dealt with in some detail.

The object of the initial adjustment is to get all four mirrors of the interferometer parallel. Before discussing the mechanics of the mirror adjustment proper, it is important to note that the mirror supports must be accurately placed. It can be shown that it is impossible to get the mirrors parallel by the following procedure if the aluminized surfaces of the mirrors are not located on the corners of a parallelogram. This adjustment was made by comparing corresponding light paths and comparing the diagonals of the square with a beam trammel until these measurements were within $\pm$ 0.005 inches of being identical. After the mirror supports have been located, the interferometer mirrors are adjusted as follows.

Mirror C (Fig. 37) is removed from the interferometer and a telescope with a Gauss eyepiece is located on the line forming the diagonal of the square of the frame and is securely fastened to the floor. Considerable care must be exercised in locating the telescope as it must be on the diagonal of the square and must also be coplanar with the interferometer support pads. After the telescope is located, mirror B is adjusted by the adjusting handles 1 and 2 (Fig. 5) until it is perpendicular to the axis of the telescope. Mirror C is then remounted in its frame and a similar adjustment is made. When this

adjustment is attained, mirrors B and C are parallel and perpendicular to the diagonal of the interferometer square.

Mirrors A and D are made parallel to mirrors B and C as follows: The mercury vapor lamp is turned on and a diaphragm having a hole one-quarter of one inch in diameter is placed as close to the lamp as possible. The collimating lens is adjusted so a parallel beam of light passes through the interferometer. A filter is placed between the collimating lens and mirror A to obtain monochromatic light and crosshairs are located at points 1 and 2 as shown in Fig. 37. An objective lens having a long focal length (24 inches) was placed as shown in Fig. 37 and focused so that an image of crosshair 1 is obtained on the screen. The distance from the objective lens to the screen was approximately eight feet, providing an enlarged image of the crosshair. Crosshair 1 is placed as close to mirror A as possible to minimize the deflection of the image of the crosshair through the light path ACD. At this stage of adjustment two images of crosshair 1 will be observed upon the screen. Each image corresponds to the light passing through one path of the interferometer. Mirror D is then adjusted until the two images coincide. The objective lens is then focused upon crosshair 2 and two images of this crosshair will be observed upon the screen. Mirror A is then adjusted until the two images merge. The objective lens is then refocused upon crosshair 1 and the process is repeated until a single image of both crosshairs is obtained without further adjustment. This process converges rapidly and as the

interferometer approaches adjustment, interference fringes should appear on the screen. The final adjustments are made visually until the whole screen is covered with one fringe. This condition can be obtained for several adjustments of the mirrors A and D. However, an optimum position can be found by observing the contrast of the fringes as the mirrors A and D are adjusted. For example, mirror A is not moved and mirror D is rotated until the maximum fringe contrast is observed. Mirror A is then adjusted in a direction so that one fringe again covers the screen. It will probably be observed that the contrast decreases as the parallel condition is approached. Mirror A is then readjusted to the condition of maximum contrast and mirror D is adjusted so as to decrease the number of fringes. This method of successive approximation is continued until the fringe of maximum contrast covers the entire field.

The fringe contrast can be further increased by adjusting the lengths of the two optical paths within the interferometer square. This is done by moving mirrors B and C parallel to the optical paths with adjusting screw 3 shown in Fig. 5. For this work this adjustment was not critical as sharp interference fringes could be obtained with a large difference in the path lengths. If the zero order fringe is desired, it can be found by introducing white light into one-half of the interferometer field. One of the mirrors is tilted so that several straight fringes are observed upon the screen. The adjusting screw 3 is then turned until the zero order fringe is observed in the "white light" half of the field.

FIGURE 37. INITIAL ADJUSTMENT OF INTERFEROMETER -

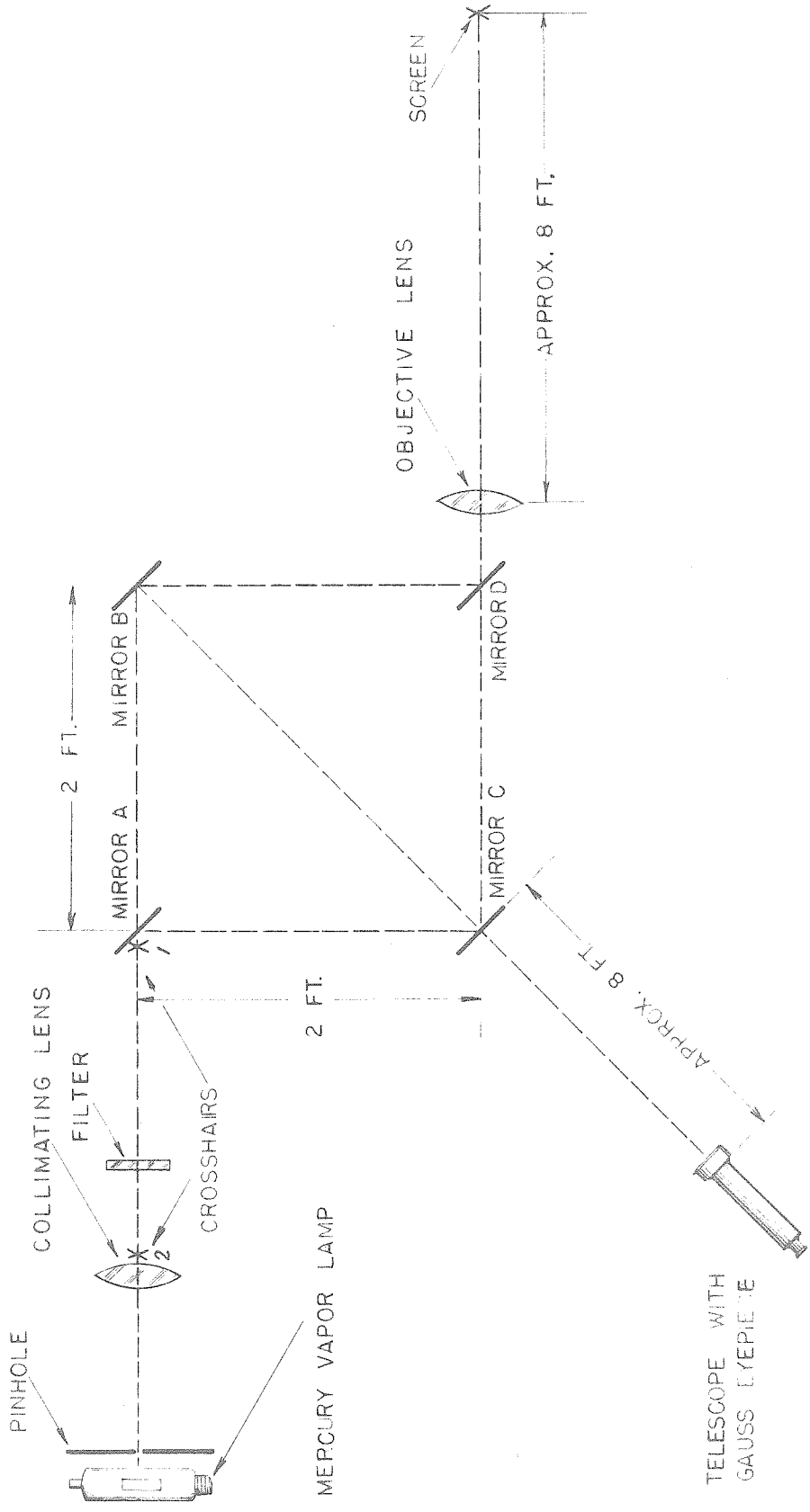

REFERENCES

(1) L. S. Kassel, "Kinetics of Homogeneous Gas Reactions", The Chemical Catalog Co., Inc., (1932).

(2) M. Bodenstein, Z. Physik Chem., (1899), Vol. 29, p. 665.

(3) K. G. Falk, J. Am. Chem. Soc., (1906), Vol. 28, p. 1517; (1907), Vol. 29, p. 536.

(4) H. B. Dixon and J. M. Crofts, J. Chem. Soc., (1914), Vol. 105, p. 2036.

(5) A. B. Dixon, L. Bradshaw, and C. Campbell, J. Chem. Soc., (1914), Vol. 105, p. 2027.

(6) C. N. Hinshelwood and Moelwyn-Hughes, Proc. Royal Society, London, (1932), Vol. A 138, p. 311.

(7) A. A. Frost and N. H. Alyea, J. Am. Chem. Soc., (1933), Vol. 55, p. 3227.

(8) L. S. Kassel and H. H. Storch, J. Am. Chem. Soc., (1935), Vol. 57, p. 672.

(9) B. Lewis and G. Von Elbe, J. Am. Chem. Soc., (1937), Vol. 59, p. 970.

(10) G. A. Cook and J. R. Bates, J. Am. Chem. Soc., (1935), Vol. 57, p. 1775.

REFERENCES (Continued)

(11) G. Von Elbe and B. Lewis, J. Chem. Phys., (1939), Vol. 7, p. 710.

(12) A. D. Allen and O. K. Rice, J. Am. Chem. Soc., (1935), Vol. 57, p. 310.

(13) H. C. Campbell and O. K. Rice, J. Am. Chem. Soc., (1935), Vol. 57, p. 1044.

(14) W. Jost and E. O. Croft, "Explosion and Combustion Processes in Gases", McGraw-Hill Book Co., Inc., New York (1946).

(15) G. Von Elbe and B. Lewis, J. Chem. Phys., (1942), Vol. 10, p. 366.

(16) J. Winkler, Review of Scientific Instruments, (1948), Vol. 19, No. 5.

(17) R. Ladenberg, J. Winkler, and C. C. Van Voorhis, The Physical Review, (1948), Vol. 73, No. 11, p. 1359.

(18) G. Joos, "Theoretical Physics", G. E. Stechert and Co., New York, (1934).

(19) International Critical Tables of Numerical Data, Physics, Chemistry and Technology, McGraw-Hill Book Co., Inc., (1926), Vol. V, p. 213.

(20) G. N. Lewis and M. Randall, "Thermodynamics and the Free Energy

REFERENCES (Continued)

of Chemical Substances", McGraw-Hill Book Co., Inc., (1923), Pgs. 485-496.

(21) F. Goldmann, Z. Physik Chem., (1929), Vol. V, Sec. b, p. 316.

(22) H. C. Hottel and H. G. Mangelsdorf, Trans. Am. Inst. of Chem. Eng., (1935), Vol. 31, No. 3.

(23) International Critical Tables of Numerical Data, Physics, Chemistry, and Technology, McGraw-Hill Book Co., Inc., (1926), Vol. V, p. 62.

(24) S. Chapman and T. G. Cowling, "The Mathematical Theory of Non-Uniform Gases", The University Press, Cambridge, (1939).

(25) A. L. Marshall, J. Am. Chem. Soc., (1927), Vol. 49, p. 2763; (1932), Vol. 54, p. 4460.

(26) International Critical Tables of Numerical Data, Physics, Chemistry, and Technology, McGraw-Hill Book Co., Inc., (1926), Vol. 7, p. 2.

(27) J. W. Mellor, "Inorganic and Theoretical Chemistry", Longmans, Green and Co., (1922), Vol. 1.

(28) W. Jost and H. O. Croft, "Explosion and Combustion Processes in Gases", McGraw-Hill Book Co., Inc., New York, (1946), p. 256.